PLOS ONE

Insights from molecular dynamics simulations: structural basis for the V567D mutation-induced instability of zebrafish alpha-dystroglycan and comparison with the murine model.

--Manuscript Draft--

Manuscript Number:	PONE-D-14-16320R1
Article Type:	Research Article
Full Title:	Insights from molecular dynamics simulations: structural basis for the V567D mutation-induced instability of zebrafish alpha-dystroglycan and comparison with the murine model.
Short Title:	In silico models of alpha-DG mutants
Corresponding Author:	Maria Cristina De Rosa Consiglio Nazionale delle Ricerche Rome, ITALY
Keywords:	Ig-like domain; molecular modelling; dystroglycan; primary dystroglycanopathies; molecular dynamics simulations
Abstract:	A missense amino acid mutation of valine to aspartic acid in 567 position of alpha-dystroglycan (DG), identified in dag1-mutated zebrafish, results in a reduced transcription and a complete absence of the protein. Lacking experimental structural data for zebrafish DG domains, the detailed mechanism for the observed mutation-induced destabilization of the DG complex and membrane damage, remained unclear. With the aim to contribute to better clarify the structure-function relationships featuring the DG complex, three-dimensional structural models of wild-type and mutant (V567D) C-terminal domain of alpha-DG from zebrafish were constructed by a template-based modelling approach. We then ran extensive molecular dynamics (MD) simulations to reveal the structural and dynamic properties of the C-terminal domain and to evaluate the effect of the single mutation on alpha-DG stability. A comparative study has been also carried out on our previously generated model of murine alpha-DG C-terminal domain including the I591D mutation, which is topologically equivalent to the V567D mutation found in zebrafish. Trajectories from MD simulations were analyzed in detail, revealing extensive structural disorder involving multiple beta-strands in the mutated variant of the protein. A biochemical analysis of the murine alpha-DG mutant I591D confirmed a pronounced instability of the protein. Taken together, the computational and biochemical analysis suggest that the V567D/I591D mutation, belonging to the G beta-strand, plays a key role in inducing a destabilization of the alpha-DG C-terminal Ig-like domain that could possibly affect and propagate to the entire DG complex. The structural features herein identified may be of crucial help to understand the molecular basis of primary dystroglycanopathies.
Order of Authors:	Davide Pirolli
	Francesca Sciandra
	Manuela Bozzi
	Bruno Giardina
	Andrea Brancaccio
	Maria Cristina De Rosa
Suggested Reviewers:	Ronen Zangi Department of Organic Chemistry I, University of the Basque Country, Spain r.zangi@ikerbasque.org
	Yunierkis Pérez-Castillo Computational Modeling Lab (CoMo), Department of Computer Sciences, Faculty of Sciences, Vrije Universiteit Brussel, Belgium yunierkis@gmail.com
	James M Kramer

	Northwestern University Feinberg School of Medicine, Feinberg Basic, Cell and Molecular Biology , Chicago, USA jkramer@northwestern.edu
Opposed Reviewers:	
Response to Reviewers:	Reviewer #1 1)"to better clarify" was changed into "a better clarification" (Line 28 of the revised manuscript). 2)As suggested by the reviewer, "Ig" definition was indicated on line 73 of the revised manuscript. 3)TM-score is a recently proposed scale for measuring the structural similarity between two structures (see Zhang and Skolnick, Scoring function for automated assessment of protein structure template quality, Proteins, 2004 57: 702-710). The purpose of proposing TM-score is to solve the problem of RMSD which is sensitive to the local error. In TM-score, the small distance is weighted stronger than the big distance which makes the score insensitive to the local modeling error. A TM-score >0.5 indicates a model of correct topology and a TM-score<0.17 means a random similarity. The TM-score values reported in Table I are parameters of the analysis performed by I-TASSER on the generated model structures. The program searches the Protein Data Bank to identify structural similarity to the predicted models and the structural similarity is quantified using TM-score. In all cases, even after the replica-exchange Monte Carlo simulations performed by I-TASSER to refine the model, 1U2C is the closest structure in the PDB and the TM-score value of 0.8 shows that the prediction is accurate. The meaning of the TM-score values, reported in Table I, was better explained (Lines 212-213 of the revised manuscript). 4)"2 times greater and lower" was changed (Line 304 of the revised manuscript). Reviewer #3 Major comment: Following the reviewer's suggestion the simulation time was doubled and an additional couple of trajectories for each protein were run (Materials and Methods of the revised manuscript, lines 141-142). This led to a significant improvement of the manuscript since our computational findings have been confirmed over three independent and longer MD simulation trajectories. It is important to outline that in the case of mutant zebrafish the observed structural instability occurs at the first frames of the MD simulation and all the RMSD, Rg and SAS values do not significantly vary in the last 30 ns of trajectory (Lines 185-194 of the revised manuscript). For sake of clarity, in the manuscript we show the results of the original MD simulation extended to 40 ns, whereas the average properties for the three simulations and the three independent Secondary Structure trajectories are reported in the Supplemental Information (Figures S2-S6). As far as murine DG is concerned a local rearrangement of Trp 549, that is tilted towards the solvent, has been demonstrated. This event, altering the forces which contribute to the conformational stability of the protein (Pace CN, Shirley BA, McNutt M, Gajiwala K. Forces contributing to the conformational stability of proteins. FASEB J. 1996, 10:75-83) may account for the reduced expression level and stability observed in the recombinant domain expressed in E. coli as well as the alteration of the maturation pathway observed in the transfected eukaryotic cells (Revised manuscript, lines 383-384). Although we believe that the important role of this topological position within the G strand of the Ig-like domain of the C-terminal region of vertebrate dystroglycans is fully confirmed, we also believe that our analysis can be considered particularly interesting and innovative in the dystroglycan field since it is showing that even if the two orthologous proteins are highly conserved, the zebrafish background and the murine one have some obvious structural differences that in the future may be useful to define some species-specific different functional behaviours. (Revised manuscript, lines 472-478). Minor comments: 1) As suggested by the reviewer the topologically equivalence between the I591D and V567D mutations is shown by sequence comparison in a novel Figure (Figure 1 of the revised manuscript). Figure numbering was modified accordingly. 2) In line 114 the word "PBD" was corrected as "PDB". 3) The Rg value of zebrafish α-DG was corrected in Table 3.

	4) Line 293: the Rg value of murine α-DG was corrected. As suggested by the Editor, the manuscript has been proofread for any possible mistake and all the amendments have been reported in the marked copy.
Additional Information:	
Question	**Response**
Financial Disclosure Please describe all sources of funding that have supported your work. A complete funding statement should do the following: Include **grant numbers and the URLs** of any funder's website. Use the full name, not acronyms, of funding institutions, and use initials to identify authors who received the funding. **Describe the role** of any sponsors or funders in the study design, data collection and analysis, decision to publish, or preparation of the manuscript. If they had no role in any of the above, include this sentence at the end of your statement: "*The funders had no role in study design, data collection and analysis, decision to publish, or preparation of the manuscript*." If the study was **unfunded**, provide a statement that clearly indicates this, for example: "*The author(s) received no specific funding for this work*." * typeset	The authors received no specific funding for this work
Competing Interests You are responsible for recognizing and disclosing on behalf of all authors any competing interest that could be perceived to bias their work, acknowledging all financial support and any other relevant financial or non-financial competing interests. Do any authors of this manuscript have competing interests (as described in the PLOS Policy on Declaration and Evaluation of Competing Interests)? **If yes**, please provide details about any and all competing interests in the box	The authors have declared that no competing interests exist

below. Your response should begin with this statement: *I have read the journal's policy and the authors of this manuscript have the following competing interests:* **If no** authors have any competing interests to declare, please enter this statement in the box: "*The authors have declared that no competing interests exist.*" * typeset	
Ethics Statement You must provide an ethics statement if your study involved human participants, specimens or tissue samples, or vertebrate animals, embryos or tissues. All information entered here should **also be included in the Methods section** of your manuscript. Please write "N/A" if your study does not require an ethics statement. **Human Subject Research (involved human participants and/or tissue)** All research involving human participants must have been approved by the authors' Institutional Review Board (IRB) or an equivalent committee, and all clinical investigation must have been conducted according to the principles expressed in the Declaration of Helsinki. Informed consent, written or oral, should also have been obtained from the participants. If no consent was given, the reason must be explained (e.g. the data were analyzed anonymously) and reported. The form of consent (written/oral), or reason for lack of consent, should be indicated in the Methods section of your manuscript. Please enter the name of the IRB or Ethics Committee that approved this study in the space below. Include the approval number and/or a statement indicating approval of this research. **Animal Research (involved vertebrate animals, embryos or tissues)** All animal work must have been	N/A

conducted according to relevant national and international guidelines. If your study involved non-human primates, you must provide details regarding animal welfare and steps taken to ameliorate suffering; this is in accordance with the recommendations of the Weatherall report, "The use of non-human primates in research." The relevant guidelines followed and the committee that approved the study should be identified in the ethics statement. If anesthesia, euthanasia or any kind of animal sacrifice is part of the study, please include briefly in your statement which substances and/or methods were applied. Please enter the name of your Institutional Animal Care and Use Committee (IACUC) or other relevant ethics board, and indicate whether they approved this research or granted a formal waiver of ethical approval. Also include an approval number if one was obtained. **Field Permit** Please indicate the name of the institution or the relevant body that granted permission.	

Dear Editor,

Thank you very much for reviewing our manuscript (PONE-D-14-16320) which has now been completely revised according to the recommendations of the reviewers. We really appreciate your suggestions which have improved the manuscript considerably.
Please find our clarifications of all the reviewer's comments in the "Response to Reviewers" file and the specific adjustments made in the revised manuscript.
We hope that the manuscript is now suitable for publication in PLoS ONE

Kind regards

Maria Cristina De Rosa

Insights from molecular dynamics simulations: structural basis for the V567D mutation-induced instability of zebrafish alpha-dystroglycan and comparison with the murine model.

Davide Pirolli[1], Francesca Sciandra[2], Manuela Bozzi[1], Bruno Giardina[1,2], Andrea Brancaccio[2*] and Maria Cristina De Rosa[2*]

[1]Istituto di Biochimica e Biochimica Clinica, Università Cattolica del Sacro Cuore and [2]Istituto di Chimica del Riconoscimento Molecolare (ICRM) - CNR c/o Università Cattolica del Sacro Cuore L.go F. Vito 1, 00168 Rome, Italy

[*]Corresponding authors contact details:

Maria Cristina De Rosa: mariacristina.derosa@icrm.cnr.it, phone: +39 06 30155135

Andrea Brancaccio: andrea.brancaccio@icrm.cnr.it, phone: +39 06 3053598

Main corresponding author: Maria Cristina De Rosa

Istituto di Chimica del Riconoscimento Molecolare - CNR

c/o Istituto di Biochimica e Biochimica Clinica, Università Cattolica del Sacro Cuore, Largo F. Vito 1, I-00168 Rome, Italy. Email: mariacristina.derosa@icrm.cnr.it.

Phone: +39 06 30155135 ; Fax: +39 06 30154309

Abstract

A missense amino acid mutation of valine to aspartic acid in 567 position of alpha-dystroglycan (DG), identified in dag1-mutated zebrafish, results in a reduced transcription and a complete absence of the protein. Lacking experimental structural data for zebrafish DG domains, the detailed mechanism for the observed mutation-induced destabilization of the DG complex and membrane damage, remained unclear. With the aim to contribute to a better clarification of the structure-function relationships featuring the DG complex, three-dimensional structural models of wild-type and mutant (V567D) C-terminal domain of alpha-DG from zebrafish were constructed by a template-based modelling approach. We then ran extensive molecular dynamics (MD) simulations to reveal the structural and dynamic properties of the C-terminal domain and to evaluate the effect of the single mutation on alpha-DG stability. A comparative study has been also carried out on our previously generated model of murine alpha-DG C-terminal domain including the I591D mutation, which is topologically equivalent to the V567D mutation found in zebrafish. Trajectories from MD simulations were analyzed in detail, revealing extensive structural disorder involving multiple beta-strands in the mutated variant of the zebrafish protein whereas local effects have been detected in the murine protein. A biochemical analysis of the murine alpha-DG mutant I591D confirmed a pronounced instability of the protein. Taken together, the computational and biochemical analysis suggest that the V567D/I591D mutation, belonging to the G beta-strand, plays a key role in inducing a destabilization of the alpha-DG C-terminal Ig-like domain that could possibly affect and propagate to the entire DG complex. The structural features herein identified may be of crucial help to understand the molecular basis of primary dystroglycanopathies.

Introduction

Dystroglycan (DG) is a pivotal member of the dystrophin-glycoprotein complex (DGC), which links the cytoskeleton to the extracellular matrix (ECM) via dystrophin [1]. Essential for normal muscle function, DG also has important roles in a wide range of tissues, including central and peripheral nervous systems, and in the maintenance of epithelial structures [2]. DG is synthesized as a precursor protein that is post-translationally cleaved into the α- and β- subunits. Within the DGC, the α-subunit is located outside the plasma membrane and binds ECM proteins, such as laminin and agrin. α-DG is extensively glycosylated and its correct glycosylation is essential to elicit its ligand binding activity [3]. Mutations in a growing number of genes encoding for glycosyltransferases or associated proteins involved in DG glycosylation give rise to a class of congenital as well as limb-girdle muscular dystrophies, which are known as secondary dystroglycanopathies [4,5]. It is worthwhile to notice that, to date, only two patients affected by recessive primary dystroglycanopathies, associated with mutations in the DG encoding gene *DAG1* (c.575C>T, T192M and c.2006G>T, C669FY) have been described [6,7].

The importance of the DG gene for muscle stability has been confirmed also in zebrafish (*Danio rerio*) [8], an organism that represents a reliable model for human muscular diseases [9–12] and that is frequently employed for investigating the effect of drugs alleviating the symptoms of Duchenne muscular dystrophy [13–15].

Recently, in an attempt to identify novel genes responsible for skeletal muscle disorders, a zebrafish mutant was identified that showed impaired locomotion behavior and dystrophic muscles [16]. Such point mutation (c.1700T>A) in *DAG1*, resulting in a missense mutation V567D, induced destabilization of the DG complex and membrane damage. In particular, genetic and biochemical studies showed that the V567D substitution is associated with a strong reduction of DG transcripts and a complete absence of α and β subunits [16]. However, despite the experimental characterization of many functional effects of the V567D substitution in α-DG, a detailed molecular framework explaining the observed destabilization and loss-of-function is still lacking.

Comprehensive details at atomic resolution about the structural perturbations induced by the V567D substitution thus remain elusive. For this reason, and given our experience with these systems, which led us to identify a second immunoglobulin-like (Ig-like) domain in murine α-DG C-terminal region [17] and ε-sarcoglycan [18], we have exploited the capabilities of molecular dynamics (MD) simulation to investigate the structural and dynamical changes of zebrafish α-DG caused by V567D replacement. In fact, we have recently predicted and then experimentally demonstrated using recombinant proteins that not only residues 60-158 of murine α-DG display an Ig-like β-sandwich fold [19], but also residues ranging from ~500 to 600 [17]. We showed that the murine α-DG C-terminal is a typical β-sandwich Ig fold consisting of two β-sheets forming a β-sandwich. The first sheet contains three anti-parallel strands (B, E, D), whereas the second sheet comprises strands A', G, F and C, with A' packing parallel with the C terminus of strand G, the others arranged in an anti-parallel fashion [20]. The zebrafish V567D substitution [16], falls within a region of α-DG which has proved to be of crucial importance to understand the role of the Ig-like domain in the interaction with the extracellular N-terminal domain of β-DG [17,21]. Gupta et al. [16], using a number of algorithms able to predict whether an amino acid substitution affects protein function, hypothesized that the V567D mutation deeply compromises protein function resulting in a pathological phenotype. Nevertheless, the structural role of this mutation remains unclear. To fill this gap, here we investigated the effects of V567D mutation on the zebrafish α-DG structure through molecular dynamics (MD) simulations, which allow the study of the conformational characteristics of the protein at every step during the computational simulations [22]. Subsequent structural *in silico* analyses were performed. Exploiting our murine α-DG model, we also examined the structural effects of the mutation I591D, which is topologically equivalent to the V567D mutation (Figure 1), combining computational and biochemical analysis.

The present MD studies revealed that the conformational stability of mutated DG is considerably reduced compared to wild-type, with a significant breakdown in the secondary structure observed

for zebrafish V567D. Potential implications in processes leading to dystroglycanopathies are discussed.

Materials and Methods

Constructing structural models of wild-type and mutant α-DG C-terminal domains

Following the same procedure used in De Rosa et al. [17] the theoretical atomic models of wild-type and mutated α-DG C-terminal regions (residues 462-626 and 483-651 for zebrafish and murine proteins, respectively) were constructed using the I-TASSER server [23,24]. Starting from the original sequence of wild-type protein retrieved from the UniProt Database [25] (accession numbers Q499B9 and Q62165 for zebrafish and murine DG, respectively), the first step I-TASSER performed was to create a sequence profile for the query using PSI-BLAST [26]. The secondary structure of each of these sequences was then predicted using PSIPRED [27], a highly accurate secondary structure prediction server (http://bioinf.cs.ucl.ac.uk/psipred). Using the constraints provided by PSI-BLAST and PSIPRED, the query was then threaded through the PDB structure library using the Local Meta-Threading-Server (LOMETS) [28], which uses eight servers to find the best possible templates for the query. The continuous fragments from the threading alignments were then excised from their respective template structures and assembled into a full-length model, whereas the unmatched regions were built via *ab initio* modelling. Hence, unlike other homology modelling software, this server predicts the structure even when there are no matched sequences in known PDB structures. The quality of each predicted structure was assessed with a scoring method, and five atomistic models with the highest scores were obtained for each input protein sequence. The best models among those predicted by I-TASSER were checked using the programs PROCHECK [29], VERIFY3D [30] and ProSA-Web (https://prosa.services.came.sbg.ac.at/prosa.php) [31]. Visualization and molecular graphics were performed using Discovery Studio (Accelrys Inc.) on the workstation HP XW8600 running Red Hat Enterprice Linux 5.

Molecular Dynamics Simulations and Analysis

The best-scored wild-type and mutant DG model structures obtained by I-TASSER were chosen as the starting coordinates for the MD simulation. Calculations were performed as reported earlier [17], with slight modifications of the size and shape of the simulation box. Briefly, all simulations were carried out using the 4.5.1 version of GROMACS [32] and GROMOS96 force field [33]. Each structure was immersed in a triclinic box with periodic boundary conditions. The SPC water model was used [34] and the systems were neutralized by 2 and 3 Na^+ ions (wild-type and mutant zebrafish, respectively) and by 3 and 2 Cl^- ions (wild-type and mutant murine, respectively). The box dimensions (7.3nm×5.6nm×8.5nm and 6.9nm×7.1nm×9.6nm for zebrafish and murine, respectively) were set to allow at least 0.9 nm between the protein and the box faces on each side. The final zebrafish systems consisted of 1671 (wild-type) and 1672 (V567D) protein atoms surrounded by 10725 and 10223 water molecules, respectively, whereas the final murine systems consisted of 1712 protein atoms (both wild-type and I591D) surrounded by 14999 and 14980 water molecules, respectively. All the MD simulations were carried out using periodic boundary conditions. The geometry of each system was initially optimized using the steepest descent algorithm and then equilibrated for 20 ps. Next, the molecular dynamics were run for 40 ns at 300 K, and the data were collected every 5 ps. Constant temperature (300 K, $\tau T = 0.1$ps) was maintained by coupling to a bath using a ν-rescale algorithm [35], whereas pressure was kept at 1 atm using the Parrinello-Rahman barostat [36]. Long range electrostatic interactions were calculated using the Particle-Mesh Ewald Method [37], whereas application of the Lincs method [38] allowed for an integration step size of 2 fs. Two additional replicate simulations with a duration of 40 ns were also performed for each of the systems studied, with differing initial velocities. Analysis of the trajectories was performed using the GROMACS tools g_rms, g_rmsf, g_hbond, g_gyrate and g_sasa. Secondary structure was calculated using the DSSP algorithm [39] within GROMACS.

DNA manipulations

The single point mutation I591D was introduced into the murine DG construct containing a myc-tag inserted within the C-terminus of α-DG and cloned in pEGFP vector [40]. The I591D mutation was

148 also introduced in a DNA construct encoding for the α-DG C-terminal domain, α-DG(485-630),
149 cloned into the pHis-Trx vector; in both cases, the QuikChange site-directed mutagenesis kit
150 (Stratagene®) was used to introduce a mutated triplet (underlined), corresponding to an Asp residue,
151 exploiting the following primers: I593D_S 5'-GTG GAT GCC TTC GAG GAC CAT GTT CAC
152 AAG CGC-3'and I593D_AS 5'-GCG CTT GTG AAC ATG GTC CTC GAA GGC ATC CAC-3'.
153 All constructs were verified by automated sequencing.
154
155 *Recombinant expression and purification of α-DG(485-630)I591D*
156 The recombinant fusion protein, 6His-Txr-α-DG(485-630), was expressed in *E.coli* BL21(DE3)
157 Codon Plus RIL strain and purified using nickel affinity chromatography as described elsewhere
158 [21]. The protein of interest, α-DG(485-630), was obtained upon thrombin cleavage. Tricine/SDS-
159 PAGE was used to check the purity of the recombinant protein under analysis.
160
161 *Cell culture, transfection and immunoprecipitation*
162 293-Ebna cells, grown in DMEM supplemented with antibiotics and 10 % (v/v) fetal calf serum,
163 were transfected with 20 μg of wild-type or I591D DG constructs using the calcium phosphate
164 method as described elsewhere [40]. After 24 h, cells were dissolved in PBS containing 1% Triton
165 X-100 and protease inhibitors (Roche, Switzerland). Cell lysate was resolved on a 10 % SDS-
166 PAGE. For Western blot analysis, proteins were transferred to nitrocellulose and probed with an
167 anti β-DG antibody (43-DAG) (1:50) and with a peroxidase-conjugated secondary antibody (Sigma,
168 USA) diluted 1:7000 (anti-mouse); the reactive products were revealed using the luminol-based
169 ECL system (Pierce, USA).
170 All the steps required for immunoprecipitation were carried out using the μMACS™ Epitope Tag
171 Protein Isolation Kit (Miltenyi Biotec.®, Germany), following the manufacturer's instructions.
172 Briefly, 1 ml of total protein extract of transfected cells was incubated with 50 μl of magnetic beads
173 conjugated with an anti-myc antibody (Miltenyi Biotec.®, Germany) for 30 min in ice. After several

washes, the adsorbed protein was eluted with 50 µl of sample buffer and run on a 10% SDS-PAGE followed by Western blot analysis with an anti-myc antibody-HRP conjugated (Miltenyi Biotec.®, Germany).

Results and discussion

The I-TASSER approach has a high success rate to construct correct folds for medium-to-large sized proteins by structurally reassembling the fragments excised from threading template structures without using homologous templates, as demonstrated by the recent CASP experiments [41,42]. In addition, we recently demonstrated the ability of the I-TASSER server to predict a reliable model of the murine α-DG C-terminal region [17]. The I-TASSER approach was therefore used to find out the secondary and tertiary structures of zebrafish wild-type and V567D α-DG C-terminus, in comparison with the murine α-DG carrying the topologically equivalent mutation I591D. Comprehensive details at atomic resolution concerning the structural perturbations induced by these amino acid substitutions were then obtained by three statistically independent MD simulations, which allowed to refine the predicted structures within a nanosecond time scale and to investigate the conformational changes, occurring upon mutation. In total, 12 MD simulations were performed as 40 ns triplicates for zebrafish wild-type, zebrafish V567D mutant, murine wild-type and murine I591D mutant. The resulting findings are very similar for each set of the three runs and here we report the results of one of the three simulations. The average properties for the three simulations, as expected similar to those of the independent simulations are reported in the Supplemental Information (Figures S2-S6). A graphical representation of secondary structure analysis for the three distinct MD simulations is shown (Fig. S4).

In silico modelling of zebrafish wild-type and V567D α-DG C-terminal region

In both systems, only β-strands and coils were found in the 475-574 region of α-DG, whereas coils, α helices and strands were found in the extreme C-terminus. Supplementary Figure S1 shows the predicted secondary structures of the two systems. Not surprisingly, the I-TASSER threading procedure identified immunoglobulin-like domains as the best templates for wild-type, specifically,

1U2C (α-DG N-terminal region [19]), 2WCP (mouse chaderin-23 [43]), 2YST (human protocadherin 7, to be published) and 3Q2V (mouse E-cadherin ectodomain [44]). The same templates, with the exception of 2YST were identified for the mutant V567D. The overall sequence identity shared between the α-DG C-terminal regions and each of the templates is approximately 24%. Although this value is quite low, it is similar to other cases in which modelling has been applied [45]. The quality of the generated models was assessed in I-TASSER based on two major criteria, the C- and the TM-scores. The C-score is calculated based on the significance of the threading alignments and the convergence of the I-TASSER simulations. C-scores typically range from -5 to 2, with higher scores reflecting a model of better quality. The TM-score is a measure of structural similarity between the predicted model and the native or experimentally determined structure, with a value > 0.5 indicating a model of correct topology. Assessments for the zebrafish α-DG C-terminal regions are reported in Table 1 indicating reasonable models and accurate topology. In all cases, search of the PDB, quantified by TM-score, indicated 1U2C as the structure with the highest structural similarity (Table I). As expected, the zebrafish α-DG model, as well as that of the V567D mutant, is similar in structure to the murine α-DG [17] with a root mean square deviation (RMSD) of the Cα atoms of 1.92Å (wild-type) and 1.68Å (V567D). According to I-TASSER then, the region encompassing residues 475-574 of the α-DG C-terminus adopts the typical I-frame immunoglobulin superfamily fold and is stabilized by extensive hydrophobic core interactions between the two β-sheets [46] (Figure 2). Consistently with the 1U2C structure and our previous results a small helix was detected between β-strands B and C (residues 495-498). The rest of the region (residues 575-626) displayed two coil-strand-coil regions separated by a helix.

To validate the computational models involved in the current study, multiple approaches were employed. Firstly, PROCHECK was used to check the stereochemistry quality and structural feature, comparing the geometry of the residues in a given protein structure with the stereochemical parameters derived from crystal or NMR structures [29]. The PROCHECK result shows that 83.6% (wild-type) and 84.2% (V567D) residues are located in favored core regions, 13.0% (wild-type)

and 12.3% (V567D) in allowed regions, 2.1% (wild-type) and 3.4% (V567D) in generously allowed regions and 1.4 % (wild-type) and 0.0% (V567D) in disallowed regions. For a good quality model, it is expected that the residues located in the most favorable and additional allowed regions should be more than 90%, which is the case for the computational structures of both wild-type and V567D α-DG C-terminal regions [47]. Residues Lys556 and Arg614 of wild-type were in disallowed region. It is worthwhile to remember here that both these residues are not located within secondary structure elements. Secondly, to further check the global quality of the computational model, the program VERIFY3D was used to analyze the compatibility of the residues with their environment [30]. Residues with a positive score should be considered reliable. In the current case, VERIFY3D result shows that 96.4% (wild-type) and 92.1% (V567D) of the residues in our computational models has an averaged 3D-1D positive score, suggesting that the model has overall self-consistency in terms of sequence-structure compatibility. The 3D–1D profile score dips below 0 at six points in the wild-type model (from Val569 to Gly573 and Ala590) and nine points in the V567D model (from Val569 to Lys577) all belonging to the unstructured region connecting the Ig-like domain with the coil-strand-coil region. ProSA (Protein Structure Analysis) [31] was adopted to further check the quality of the generated models. The Z-scores, a parameter describing the overall model quality, are predicted to be -4.5 and -4.6 for wild-type and V567D structure model, respectively. Both values are within the range of Z-scores found for native proteins of similar size, indicating that the overall quality of our model is high. A summary of the results obtained from these programs, indicating that the residues in the model are placed in a very good overall configuration, is reported in Table 2.

In silico modelling of murine I591D α-DG C-terminal region

Primary sequence and secondary structure prediction by I-TASSER of murine wild-type and I591D α-DG C-terminal region are shown in Supplementary Figure S1. Analogously to the zebrafish DG, only β-strands and coils were predicted in the secondary structure of the region spanning residues 500-600, whereas coils, α helices and strands were found in the extreme C-terminus. The I-

TASSER server used the crystal structure of the murine α-DG N-terminal domain (PDB 1U2C [19]) and of mouse E-cadherin ectodomain (PDB 3Q2V [48]) as template structures to assemble the model of the I591D C-terminal domain of murine α-DG. Statistical support for the predicted structural models is reported in Table I. The two major criteria, the C-score and the TM-score, indicate reasonable models with very similar overall topology and a high degree of three-dimensional structure similarity. As expected, according to I-TASSER, the model of the I591D α-DG C-terminus is similar in structure to 1U2C (Cα RMSD = 1.73 Å) and consists of an Ig-like domain (residues 500–600) and a coil–helix–coil region (601-653). The structure and topology of the mutant murine Ig-like domain closely resemble those of the wild-type [17] and of the predicted zebrafish Ig-like (Figure 2).

Analysis using PROCHECK [29] indicates excellent geometry with no residues in disallowed regions of the Ramachandran plot. 87.6%, 11.0% and 1.4% of the residues fall into the favored core, allowed, and generously allowed regions, respectively. For the most representative structure VERIFY3D and ProSA profiles also are indicative of a high quality model. In the VERIFY3D scan, the designed model shows that all the residues have an average 3D-1D positive score with the exception of Pro614, which is however located in the predicted random coil region in the extreme C-terminus. A ProSA Z-score of -4.5 also confirms the good quality of the model. Assessment of the three-dimensional model is summarized in Table 2.

Molecular dynamics conformational flexibility and stability analysis

To check the stability of the simulations, the RMSDs of the Cα atoms with respect to the minimized starting structure, radii of gyration (Rg) of the protein and Solvent Accessible Surface Area (SASA) of protein were calculated and monitored over the course of simulations and are presented in Figure 3. Evaluation of the structural drift was provided by the analysis of the Cα atom RMSDs from the initial structures as a function of time. The RMSDs of the Ig-like domains through the 40 ns trajectory were computed with respect to their corresponding initial minimized structures (Fig. 3A).

In all four cases, the RMSD shows convergence of the simulation within 40 ns (Fig. 3A). The wild-type murine protein presents the smallest deviation and adopted after 200 ps a stable conformation not so far from the initial one (0.1 nm), indicating that this system was very stable during the simulation. The RMSD of wild-type zebrafish simulation converges after 10 ns to a value around 0.24 nm, whereas in the mutants simulations RMSD increases sharply till 1 ns and reaches a value of 0.20 nm (zebrafish V567D) and 0.17 nm (murine I591D) remaining reasonably stable until the end of the simulation (Fig. 3A). Figure 3 demonstrates that for all structures, the RMSD remains stable around average values of 0.1-0.2 nm (Table 3) over a considerable time period (30 ns) of the later part of the trajectory. The SASA and Rg are related to (and give a global account of) the general tertiary structure of the protein. The curves of $SASA_{TOTAL}$ indicate that the exposed areas (both hydrophobic and hydrophilic), for all the systems investigated, although slightly decreasing with the mutation (an effect more evident in the case of zebrafish), are stable during the entire simulations (Fig. 3B). As expected from the RMSD analysis, it is not possible to observe significant changes in the Rg during the simulations. The plot of Rg versus time is presented in Fig. 3C. For both zebrafish and murine systems the curves do not differ significantly and maintain the lowest value of Rg around ~1.3 nm (zebrafish) and ~1.5 nm (murine), indicating that the compact conformation is largely preserved upon mutation (Fig. 3C). The time averaged structural properties are reported in Table 3.

Interesting information comes from the root mean square fluctuations (RMSFs) of each amino acid (Fig. 4), which highlights the flexible regions of the systems. RMSFs values higher than 0.25 nm are characteristic of amino acid residues belonging to flexible regions. For all the systems analysed, the loop at the N-terminus and the loops between the β-strands displayed RMSFs values which are typical of flexible regions, while the regular secondary structure regions showed small fluctuations during the simulations. In the zebrafish DG, the most pronounced Cα-RMSF differences between the wild-type and the mutant occur for residues 500-502 and 517-519, which belong to the long loops connecting strands B and C, and C and D, respectively (Fig. 4A). In these two regions the

V567D Cα-RMSF is ~1.5 and ~2 times larger than that of the wild-type, respectively. The RMSFs values observed for murine DG exhibit more or less similarly distributed fluctuations. Most of the residues, which belong to the loops connecting strands C and D, D and E, F and G, become highly mobile upon mutation (Fig. 4B).

We then tried to examine whether the mutation induced any changes in the secondary structural elements during the simulations. Fig. 5 shows the classification of the four trajectories in terms of secondary-structure elements obtained by the software tool DSSP [39], whose plots enable a local structural analysis complementing the above characterization of the dynamics. The stability of the secondary structures was examined during the entire period (40 ns) (Fig. 5). Interestingly, among the four simulated systems, the V567D zebrafish shows a strong disorganization of strand A' (Fig. 5B), a phenomenon not observed in the other models, whose secondary structure elements appeared very stable during the entire MD simulations. Examination of Figure 5 shows that the main features of the β-sheets structure are largely retained, i.e., the strands A', G, F, C, and the others B, E, D are preserved throughout the 40-ns simulation for wild-type zebrafish (Fig. 5A), wild-type murine (Fig. 5C) and I591D murine α-DG (Fig. 5D). By contrast, at 0.1 ns of the V567D simulation, most of the A' strand unfolds and is converted into loop giving rise to a long flexible region at the N-terminus of the domain (Fig. 5B). Large scale fluctuations from helical to bend or turn structures at the long loop connecting strands B and C are observed in all the systems (Fig. 5).

Effects of V567D and I591D substitutions on the stability of the Ig-fold

The Ig-like domain is stabilized by hydrophobic core interactions between the two β-sheets and by the hydrogen bonds between the β-strands [39,49]. Interfering with any of the residues in the sheet by a mutation may lead to a discontinuity in the hydrogen bonding pattern, which is characteristic of the Ig-like domains. This may enhance the conformational flexibility of the mutated residue side chain, which could disrupt the natural bonding of neighbours and might result in loss of secondary structural elements [50,51]. The external strands A' and G present geometrical distortions known

as β-bulges, as found in some Ig molecules [52], which lead to an imperfect general H-bond network. However, examination of the hydrogen bond patterns involving the β-strands A'-G reveals significant differences among the simulated systems (Fig. 6). Figure 6A shows that the backbone hydrogen bonds formed between the strands A' and G, where the mutation is located, are stable in zebrafish wild-type but are disrupted in the zebrafish V567D mutant, resulting in a significant separation between the two strands in the β-sheet. By contrast, the corresponding backbone hydrogen bonds in murine DG were not noticeably affected by the I591D mutation (Fig. 6B). The changes in the hydrogen bond pattern observed in zebrafish DG are closely related to the disruption of the native hydrophobic contacts. Val567 residue, located on the G strand, interacts with a number of hydrophobic residues nearby and the strongest interactions are observed with Val481(β-strand A'), Ala483(β-strand A'), Phe489 (β-strand B) and Val491 (β-strand B). Significantly, unlike Val567, the acidic Asp567 residue of mutant DG maintains its side chain exposed to the solvent over the simulation time. Analysis of the MD trajectories shows that the hydrophobic contacts involving the 567 position remain relatively stable in the wild-type with the Val567 residue continuously interacting with residues Val481, Phe489, Ala483 and Val491 whereas they are disrupted upon mutation. This results in a significant disorganization of the A' strand and in a widening of the cleft between the sheets of the Ig-like domain. This effect is not observed in murine α-DG, in which the hydrophobic contacts established by Ile591 with Val504, Ala506, Phe512 and Val514 are well preserved after the mutation. The Cα-Cα distances between the above-mentioned residues are reported in Fig. 7 for both, zebrafish (A, C, E and G panels) and murine (B, D, F, and H panels) protein models, in comparison with their mutated counterpart. Panels A, C, E and G highlight the separation between A'-G (Fig. 7A, C) and B-G (Fig. 7E, G) strands. Notably, the large differences observed between Cα of 489, 491 (strand B) and 567 (strand A') positions (Figure 7E, G) indicate the separation between the two sheets of the β-sandwich (Fig. 2). In the case of murine α-DG the I591D replacement produces no effect on the corresponding distances between A'-G (Fig. 7B, D) strands and very little effects on the separation between the sheets (Fig. 7F, H).

356 We also examined the structural conformations obtained from the MD simulations of the wild-type
357 and the mutant α-DG to better evaluate the conformational change in the mutant protein upon the
358 amino acid replacement. Structural comparison between the average structures generated from the
359 last 25 ns MD trajectory is shown in Figure 8. TM-score can be used as an approximate but
360 quantitative criterion for protein topology classification, i.e. protein pairs with a TM-score >0.5 are
361 mostly in the same fold, while those with a TM-score <0.5 are mainly not in the same fold [53,54].
362 A TM-score of 0.55 and 0.71 were calculated for zebrafish and murine average structures,
363 respectively, indicative of a low similarity between the wild-type and the mutant zebrafish protein.
364 As shown in Figure 8 the V567D substitution causes the unfolding of the A strand and the G strand
365 pulling away from the β-sheet (Figure 8A, B). As a result, the two β-sheets slide away from each
366 other and the average distance between the center of mass of B and G strands increases from 10.3 Å
367 (wild-type) to 14.8 Å (V567D) (Figure 8A, B). The extent of the mutation-induced structural
368 rearrangement can also be seen from the changes in the solvent exposure of the groups interacting
369 with the mutation site. The segment that becomes more exposed to the solvent upon V567D
370 mutation is the B-strand (36% SASA increase). Notably, we observed a significant increase in
371 SASA of Val491 whose value is 14 $Å^2$ in wild-type and 32 $Å^2$ in V567D, in agreement with the
372 analysis of Halaby and coworkers [49], who calculated, for amino acids of the internal strand B
373 with side chains pointing towards the interior of the protein, a SASA value < 20 $Å^2$ and for amino
374 acids with side chains pointing towards the exterior of the protein SASA values between 20 $Å^2$ and
375 50 $Å^2$. In the wild-type and I591D murine average structures, we focused on the D-strand which
376 appears as the most affected region upon mutation. The strong hydrophobic interactions involving
377 Ile591 and Trp549 (D strand) in wild-type murine α-DG are shown in Figure 8C. Notably, the
378 SASA analysis shows that there is a drastic increase in SASA for Trp549, from 18 $Å^2$ (wild-type) to
379 45 $Å^2$ (I591D), values that are in reasonable agreement with the SASA values expected for residues
380 of an external strand as the strand D [49]. These changes are possibly triggered by the amino acid
381 replacement at Ile591 position, which affected the normal interactions between Ile591 and Trp549.

Effectively, in the mutant murine DG the Asp591 side chain forms an hydrogen bond with Ser548 and this results in the movement of the indole ring belonging to Trp549 towards the solvent (Figure 8D), an event that might induce a significant destabilization [55]. On the whole, the establishment of new contacts that remain stable during the simulation suggests that the Ig-like domain of murine α-DG should not display an impaired stability when Ile591 is replaced by Asp. Nevertheless, possible structural-functional consequences derived from the observed structural rearrangement cannot be ruled out as indicated by our analysis of the recombinant protein carrying the I591D mutation (see below).

Preparation of the recombinant murine α-DG(485-630)I591D mutant

In order to test the stability of the mutant α-DG C-terminal domain, namely α-DG(485-630)I591D, we prepared this construct using our consolidated prokaryotic expression system (*E. coli*) that we have previously used for analyzing a plethora of murine domains of DG [21].

The recombinant mutant α-DG(485-630)I591D, expressed as a fusion protein conjugated with six N-terminal histidine residues and the thioredoxin (Trx), was purified by affinity chromatography using a nickel nitrilotriacetate resin. After thrombin cleavage to separate α-DG(485-630)I591D from its fusion partner, the protein was submitted to a further affinity chromatography step to remove the fusion partner from the solution. A similar protocol was applied to the wild-type protein in order to compare the stability of the two proteins (Fig. 9). Any attempt made to further purify the I591D mutant was unsuccessful because of its high propensity to degradation. Figure 9 shows an SDS-PAGE, in which protein samples at different stages of the purification protocol were analyzed. The purified protein, compared to its wild-type counterpart, displays a faint band corresponding to the lower degraded band observed in the wild-type, while no signal corresponding to the full-length protein can be observed. At the present stage, due to this pronounced unstable behavior, it is actually impossible to collect significant amounts of the I591D variant to be employed for its biochemical characterization.

Analysis of the expression of the mutant I591D in transfected 293-Ebna cells

We further assessed the effects of the I591D mutation *in vitro*, with respect to expression and post-translational processing of DG. To this end, we transiently expressed the full-length wild-type and I591D DG proteins in 293-Ebna cells using two DNA constructs carrying a myc-tag inserted at the position K498 of the C-terminal domain of α-DG and cloned in a pEGFP vector [40].

Interestingly, the mutation does not prevent or downregulate the expression of DG compared to the wild-type, however the structural rearrangements occurring in I591D partially impair the post-translational cleavage of the mutated DG precursor. In fact, an additional band at about 160 kDa is detected in Western blot using anti β-DG or anti-myc antibodies (Fig. 10 A and B). It was already shown that mutations that affect the stability of the DG precursor, such as the disruption of disulfide bridge within the extracellular domain of β-DG or the perturbation of the interaction between the two subunits, strongly influence its post-translational cleavage and plasma membrane targeting [21,56,57].

Conclusions

Understanding the molecular consequences of the mutations that cause human genetic diseases remains an important research challenge. Missense mutations may have diverse structural and functional effects on proteins, ranging from changes in the folding pathway that may affect their overall stability, to alterations in their ligand binding properties. Computational methods have been widely used to assess the structural effects of genetic variants and to investigate the detailed mechanisms underlying the pathogenicity of missense mutations.

Given our previous biochemical and computational work on the C-terminal region of α-DG [17,21], it was of great interest for us that a recently discovered point mutation (c.1700T>A) in the gene *DAG1* of zebrafish, resulting in the V567D missense mutation, could induce a very strong destabilization of the protein eventually leading to the absence of protein and to a reduction of its mRNA levels [16].

In this study, the impact of the single amino acid substitution V567D on the stability of α-DG was evaluated combining a number of computational methods to improve prediction. Our findings provide new insights into the structural basis for the reported dramatic destabilization of zebrafish DG induced by the V567D mutation and gives a possible molecular explanation to understand how the homologous and topologically related I591D mutation in murine DG could also compromise the protein function. The presence of a hydrophobic residue in this position, such as a Val or Ile, is highly conserved within all the DG sequences so far analyzed [21]. Although belonging to an external strand (G), these residues are also involved in forming hydrophobic interactions with the internal core of the Ig-like domain. We have shown that Val567 residue plays a pivotal role in maintaining the hydrophobic core structure of the Ig-like domain. By a set of molecular dynamics simulations, in which the dynamics of wild-type and mutated DG were compared, evident signs of stability loss provoked by the V567D mutation were observed in the number of hydrogen bonds, hydrophobic contacts and inter-strand packing distances between the β-sheets of the Ig-fold. The local perturbation at the G-strand may function as a nucleation site for the unfolding of the protein

448 and account for the experimentally observed destabilization [16]. We can hypothesize that in
449 zebrafish the severe perturbation of the central hydrophobic core structure of the Ig folded-domain
450 prevents the correct folding of the DG precursor impairing its entire maturation and targeting
451 pathway, in line with the accepted idea that the central core of the Ig fold serves as a scaffold for the
452 presentation of sites involved in molecular recognition, cell adhesion, and ligand binding [58,59].
453 In the case of I591D murine DG, important conformational changes were found to occur within a
454 short time, **s**uggesting potential changes from the native structural properties within this protein
455 region. Although we found that the I591D mutation is not likely to change the overall stability or
456 dynamics of the entire protein region and in particular of the Ig-like domain, however, it brings
457 about a significant local perturbation featuring the exposure of Trp549 towards the solvent. Namely,
458 the D strand dynamicsvaries in a way that may still suggest a disturbance to the structural integrity
459 of the domain. This event may account for the reduced expression level and stability of the
460 recombinant domain expressed in *E. coli* and the alteration of the maturation pathway observed in
461 the transfected eukaryotic cells. On the whole, theoretical and experimental findings demonstrated
462 that the I591D mutation can affect several biophysical characteristics simultaneously and it may
463 therefore lead to a certain degree of instability as indicated by the high propensity to degradation
464 displayed by the recombinant α-DG C-terminal domain (see Fig. 9) and by the altered maturation
465 pathway of DG, observed in our experiments using transfected cells (see Fig. 10).
466 The reduced affinity displayed by hypoglycosylated DG towards laminin is believed to represent
467 the major molecular clue behind a number of secondary dystroglycanopathies [60], while much less
468 is currently known on the molecular mechanism behind the two known primary
469 dystroglycanopathies [6,7]. It is interesting to note that the V567D/I591D mutation affects a domain
470 of α-DG which is not extensively glycosylated. Only a few Thr residues within the loop
471 interconnecting B and C strands were reported as GalNAc glycosylation sites and in particular the
472 G strand, to which V567D/I591D belongs, was found unglycosylated [61]. Although we believe
473 that the important role of this topological position within the G strand of the Ig-like domain of the

C-terminal region of vertebrate dystroglycans is fully confirmed, we also believe that our analysis can be considered particularly interesting and innovative in the dystroglycan field since it is showing that even if the two orthologous proteins are highly conserved, the zebrafish background and the murine one have some obvious structural differences that in the future may be useful to define some species-specific different functional behaviours. In order to enlarge our knowledge on primary dystroglycanopathies, in the next future it will be more and more important to consider that also mutations affecting folding, stability and maturation of the DG precursor can lead to severe neuromuscular conditions as well as those affecting DG glycosylation's shell. Our study reinforces the notion of the importance of a combined computational and biochemical approach for the study of complex diseases such as dystroglycanopathies.

Acknowledgments

The authors would like to thank Elena Gonnelli for her technical assistance.

References

1. Henry MD, Campbell KP (1999) Dystroglycan inside and out. Curr Opin Cell Biol 11: 602–607.

2. Durbeej M, Henry MD, Campbell KP (1998) Dystroglycan in development and disease. Curr Opin Cell Biol 10: 594–601.

3. Muntoni F, Torelli S, Wells DJ, Brown SC (2011) Muscular dystrophies due to glycosylation defects: diagnosis and therapeutic strategies. Curr Opin Neurol 24: 437–442. doi:10.1097/WCO.0b013e32834a95e3.

4. Muntoni F, Brockington M, Brown SC (2004) Glycosylation eases muscular dystrophy. Nat Med 10: 676–677. doi:10.1038/nm0704-676.

5. Godfrey C, Clement E, Mein R, Brockington M, Smith J, et al. (2007) Refining genotype - phenotype correlations in muscular dystrophies with defective glycosylation of dystroglycan. Brain 130: 2725–2735. doi:10.1093/Brain/Awm212.

6. Hara Y, Balci-Hayta B, Yoshida-Moriguchi T, Kanagawa M, Beltran-Valero de Bernabe D, et al. (2011) A dystroglycan mutation associated with limb-girdle muscular dystrophy. N Engl J Med 364: 939–946. doi:10.1056/NEJMoa1006939.

7. Geis T, Marquard K, Rödl T, Reihle C, Schirmer S, et al. (2013) Homozygous dystroglycan mutation associated with a novel muscle–eye–brain disease-like phenotype with multicystic leucodystrophy. Neurogenetics 14: 205–213. doi:10.1007/s10048-013-0374-9.

8. Parsons MJ, Campos I, Hirst EMA, Stemple DL (2002) Removal of dystroglycan causes severe muscular dystrophy in zebrafish embryos. Dev Camb Engl 129: 3505–3512.

9. Guyon JR, Steffen LS, Howell MH, Pusack TJ, Lawrence C, et al. (2007) Modeling human muscle disease in zebrafish. Biochim Biophys Acta 1772: 205–215. doi:10.1016/j.bbadis.2006.07.003.

10. Kawahara G, Guyon JR, Nakamura Y, Kunkel LM (2010) Zebrafish models for human FKRP muscular dystrophies. Hum Mol Genet 19: 623–633. doi:10.1093/hmg/ddp528.

11. Wood AJ, Müller JS, Jepson CD, Laval SH, Lochmüller H, et al. (2011) Abnormal vascular development in zebrafish models for fukutin and FKRP deficiency. Hum Mol Genet 20: 4879–4890. doi:10.1093/hmg/ddr426.

12. Moore CJ, Goh HT, Hewitt JE (2008) Genes required for functional glycosylation of dystroglycan are conserved in zebrafish. Genomics 92: 159–167. doi:10.1016/j.ygeno.2008.05.008.

13. Winder SJ, Lipscomb L, Angela Parkin C, Juusola M (2011) The proteasomal inhibitor MG132 prevents muscular dystrophy in zebrafish. PLoS Curr 3: RRN1286. doi:10.1371/currents.RRN1286.

14. Kawahara G, Kunkel LM (2013) Zebrafish based small molecule screens for novel DMD drugs. Drug Discov Today Technol 10: e91–96. doi:10.1016/j.ddtec.2012.03.001.

15. Johnson NM, Farr GH 3rd, Maves L (2013) The HDAC Inhibitor TSA Ameliorates a Zebrafish Model of Duchenne Muscular Dystrophy. PLoS Curr 5. doi:10.1371/currents.md.8273cf41db10e2d15dd3ab827cb4b027.

16. Gupta V, Kawahara G, Gundry SR, Chen AT, Lencer WI, et al. (2011) The zebrafish dag1 mutant: a novel genetic model for dystroglycanopathies. Hum Mol Genet 20: 1712–1725. doi:10.1093/hmg/ddr047.

17. De Rosa MC, Pirolli D, Bozzi M, Sciandra F, Giardina B, et al. (2011) A second Ig-like domain identified in dystroglycan by molecular modelling and dynamics. J Mol Graph Model 29: 1015–1024. doi:10.1016/j.jmgm.2011.04.008.

18. Waite A, De Rosa MC, Brancaccio A, Blake DJ (2011) A gain-of-glycosylation mutation associated with myoclonus-dystonia syndrome affects trafficking and processing of mouse ε-sarcoglycan in the late secretory pathway. Hum Mutat 32: 1246–1258. doi:10.1002/humu.21561.

19. Bozic D, Sciandra F, Lamba D, Brancaccio A (2004) The structure of the N-terminal region of murine skeletal muscle alpha-dystroglycan discloses a modular architecture. J Biol Chem 279: 44812–44816. doi:10.1074/jbc.C400353200.

20. Bork P, Holm L, Sander C (1994) The immunoglobulin fold. Structural classification, sequence patterns and common core. J Mol Biol 242: 309–320. doi:10.1006/jmbi.1994.1582.

21. Sciandra F, Bozzi M, Morlacchi S, Galtieri A, Giardina B, et al. (2009) Mutagenesis at the α-β interface impairs the cleavage of the dystroglycan precursor: Mutagenesis induces an uncleaved dystroglycan. FEBS J 276: 4933–4945. doi:10.1111/j.1742-4658.2009.07196.x.

22. Daggett V, Levitt M (1993) Realistic simulations of native-protein dynamics in solution and beyond. Annu Rev Biophys Biomol Struct 22: 353–380. doi:10.1146/annurev.bb.22.060193.002033.

23. Zhang Y (2008) I-TASSER server for protein 3D structure prediction. BMC Bioinformatics 9: 40. doi:10.1186/1471-2105-9-40.

24. Wu S, Skolnick J, Zhang Y (2007) Ab initio modeling of small proteins by iterative TASSER simulations. BMC Biol 5: 17. doi:10.1186/1741-7007-5-17.

25. Jain E, Bairoch A, Duvaud S, Phan I, Redaschi N, et al. (2009) Infrastructure for the life sciences: design and implementation of the UniProt website. BMC Bioinformatics 10: 136. doi:10.1186/1471-2105-10-136.

26. Altschul SF, Madden TL, Schaffer AA, Zhang J, Zhang Z, et al. (1997) Gapped BLAST and PSI-BLAST: a new generation of protein database search programs. Nucleic Acids Res 25: 3389–3402.

27. McGuffin LJ, Bryson K, Jones DT (2000) The PSIPRED protein structure prediction server. Bioinformatics 16: 404–405.

28. Wu S, Zhang Y (2007) LOMETS: a local meta-threading-server for protein structure prediction. Nucleic Acids Res 35: 3375–3382. doi:10.1093/nar/gkm251.

562 29. Morris AL, MacArthur MW, Hutchinson EG, Thornton JM (1992) Stereochemical quality of
563 protein structure coordinates. Proteins 12: 345–364. doi:10.1002/prot.340120407.

564 30. Luthy R, Bowie JU, Eisenberg D (1992) Assessment of protein models with three-dimensional
565 profiles. Nature 356: 83–85. doi:10.1038/356083a0.

566 31. Wiederstein M, Sippl MJ (2007) ProSA-web: interactive web service for the recognition of
567 errors in three-dimensional structures of proteins. Nucleic Acids Res 35: W407–10.
568 doi:10.1093/nar/gkm290.

569 32. Van Der Spoel D, Lindahl E, Hess B, Groenhof G, Mark AE, et al. (2005) GROMACS: fast,
570 flexible, and free. J Comput Chem 26: 1701–1718. doi:10.1002/jcc.20291.

571 33. Stocker U, van Gunsteren WF (2000) Molecular dynamics simulation of hen egg white
572 lysozyme: a test of the GROMOS96 force field against nuclear magnetic resonance data.
573 Proteins 40: 145–153.

574 34. Hermans J, Berendsen HJC, Vangunsteren WF, Postma JPM (1984) A Consistent Empirical
575 Potential for Water-Protein Interactions. Biopolymers 23: 1513–1518.
576 doi:10.1002/bip.360230807.

577 35. Bussi G, Donadio D, Parrinello M (2007) Canonical sampling through velocity rescaling. J
578 Chem Phys 126: 014101. doi:10.1063/1.2408420.

579 36. Parrinello M, Rahman A (1981) Polymorphic Transitions in Single-Crystals: a New Molecular-
580 Dynamics Method. J Appl Phys 52: 7182–7190. doi:10.1063/1.328693.

581 37. Darden T, York D, Pedersen L (1993) Particle Mesh Ewald - an N.Log(N) Method for Ewald
582 Sums in Large Systems. J Chem Phys 98: 10089–10092. doi:10.1063/1.464397.

583 38. Hess B, Bekker H, Berendsen HJC, Fraaije JGEM (1997) LINCS: A linear constraint solver for
584 molecular simulations. J Comput Chem 18: 1463–1472. doi:10.1002/(Sici)1096-
585 987x(199709)18:12<1463::Aid-Jcc4>3.0.Co;2-H.

586 39. Kabsch W, Sander C (1983) Dictionary of protein secondary structure: pattern recognition of
587 hydrogen-bonded and geometrical features. Biopolymers 22: 2577–2637.
588 doi:10.1002/bip.360221211.

589 40. Morlacchi S, Sciandra F, Bigotti M, Bozzi M, Hübner W, et al. (2012) Insertion of a myc-tag
590 within α-dystroglycan domains improves its biochemical and microscopic detection. BMC
591 Biochem 13: 14. doi:10.1186/1471-2091-13-14.

592 41. Xu D, Zhang J, Roy A, Zhang Y (2011) Automated protein structure modeling in CASP9 by I-
593 TASSER pipeline combined with QUARK-based ab initio folding and FG-MD-based structure
594 refinement. Proteins Struct Funct Bioinforma 79: 147–160. doi:10.1002/prot.23111.

595 42. Zhang Y (2013) Interplay of I-TASSER and QUARK for template-based and ab initio protein
596 structure prediction in CASP10: Composite Protein Structure Prediction in CASP10. Proteins
597 Struct Funct Bioinforma: n/a–n/a. doi:10.1002/prot.24341.

598 43. Sotomayor M, Weihofen WA, Gaudet R, Corey DP (2010) Structural determinants of cadherin-
599 23 function in hearing and deafness. Neuron 66: 85–100. doi:10.1016/j.neuron.2010.03.028.

600 44. Harrison OJ, Jin X, Hong S, Bahna F, Ahlsen G, et al. (2011) The extracellular architecture of
601 adherens junctions revealed by crystal structures of type I cadherins. Structure 19: 244–256.
602 doi:10.1016/j.str.2010.11.016.

603 45. Bissantz C, Bernard P, Hibert M, Rognan D (2003) Protein-based virtual screening of chemical
604 databases. II. Are homology models of G-Protein Coupled Receptors suitable targets? Proteins
605 50: 5–25. doi:10.1002/prot.10237.

606 46. Harpaz Y, Chothia C (1994) Many of the immunoglobulin superfamily domains in cell
607 adhesion molecules and surface receptors belong to a new structural set which is close to that
608 containing variable domains. J Mol Biol 238: 528–539. doi:10.1006/jmbi.1994.1312.

609 47. Wang J-F, Chou K-C (2012) Insights into the Mutation-Induced HHH Syndrome from
610 Modeling Human Mitochondrial Ornithine Transporter-1. PLoS ONE 7: e31048.
611 doi:10.1371/journal.pone.0031048.

612 48. Harrison OJ, Jin X, Hong S, Bahna F, Ahlsen G, et al. (2011) The extracellular architecture of
613 adherens junctions revealed by crystal structures of type I cadherins. Structure 19: 244–256.
614 doi:10.1016/j.str.2010.11.016.

615 49. Halaby DM, Poupon A, Mornon J-P (1999) The immunoglobulin fold family: sequence analysis
616 and 3D structure comparisons. Protein Eng Des Sel 12: 563–571. doi:10.1093/protein/12.7.563.

617 50. Gajendrarao P, Krishnamoorthy N, Kassem HS, Moharem-Elgamal S, Cecchi F, et al. (2013)
618 Molecular Modeling of Disease Causing Mutations in Domain C1 of cMyBP-C. PLoS ONE 8:
619 e59206. doi:10.1371/journal.pone.0059206.

620 51. Ababou A, Rostkova E, Mistry S, Masurier CL, Gautel M, et al. (2008) Myosin Binding Protein
621 C Positioned to Play a Key Role in Regulation of Muscle Contraction: Structure and
622 Interactions of Domain C1. J Mol Biol 384: 615–630. doi:10.1016/j.jmb.2008.09.065.

623 52. Chan AW, Hutchinson EG, Harris D, Thornton JM (1993) Identification, classification, and
624 analysis of beta-bulges in proteins. Protein Sci Publ Protein Soc 2: 1574–1590.
625 doi:10.1002/pro.5560021004.

626 53. Zhang Y, Skolnick J (2004) Scoring function for automated assessment of protein structure
627 template quality. Proteins 57: 702–710. doi:10.1002/prot.20264.

628 54. Xu J, Zhang Y (2010) How significant is a protein structure similarity with TM-score = 0.5?
629 Bioinforma Oxf Engl 26: 889–895. doi:10.1093/bioinformatics/btq066.

630 55. Pace CN, Shirley BA, McNutt M, Gajiwala K (1996) Forces contributing to the conformational
631 stability of proteins. FASEB J Off Publ Fed Am Soc Exp Biol 10: 75–83.

632 56. Watanabe N, Sasaoka T, Noguchi S, Nishino I, Tanaka T (2007) Cys669-Cys713 disulfide
633 bridge formation is a key to dystroglycan cleavage and subunit association. Genes Cells 12: 75–
634 88. doi:10.1111/j.1365-2443.2006.01033.x.

635 57. Sciandra F, Angelucci E, Altieri F, Ricci D, Hübner W, et al. (2012) Dystroglycan is associated
636 to the disulfide isomerase ERp57. Exp Cell Res 318: 2460–2469.
637 doi:10.1016/j.yexcr.2012.07.006.

638 58. Halaby DM, Mornon JPE (1998) The immunoglobulin superfamily: An insight on its tissular,
639 species, and functional diversity. J Mol Evol 46: 389–400. doi:10.1007/PL00006318.

640 59. McCormick KA (1998) Molecular Determinants of Na+ Channel Function in the Extracellular
641 Domain of the beta 1 Subunit. J Biol Chem 273: 3954–3962. doi:10.1074/jbc.273.7.3954.

642 60. Sciandra F, Bozzi M, Bigotti MG, Brancaccio A (2013) The multiple affinities of α-
643 dystroglycan. Curr Protein Pept Sci 14: 626–634.

644 61. Harrison R, Hitchen PG, Panico M, Morris HR, Mekhaiel D, et al. (2012) Glycoproteomic
645 characterization of recombinant mouse α-dystroglycan. Glycobiology 22: 662–675.
646 doi:10.1093/glycob/cws002.

647

Table 1. Statistical support for the predicted structural models obtained from I-TASSER.

α-DG	**Quality of Predicted Model**	
	C-score	**TM-Score**[a]
Wild-type zebrafish	-0.8	0.8
V567D zebrafish	-0.9	0.8
Wild type murine	-0.7	0.8
I591D murine	-0.6	0.8

[a]Calculated with respect to the closest structure in the PDB (1U2C)

651 **Table 2**. Evaluation of I-TASSER models by using PROCHECK, ProSA-Web and VERIFY3D

652 protein structure evaluation tools.

α-DG	**PROCHECK**				**VERIFY3D**	**ProSA**
	Ramachandran plot statistics (%)[(a)]					
	Core	**Allowed**	**General**	**Disallowed**	**Compatibiliy score (%)[(b)]**	**z-score**
Wild-type zebrafish	83.6	13.0	2.1	1.4	96.4	-4.5
V567D zebrafish	84.2	12.3	3.4	-	92.1	-4.6
Wild-type murine[c]	94.5	4.8	-	-	100.0	-5.4
I591D murine	87.6	11.0	1.4	-	99.4	-4.5

653 [a]Ramachandran plot qualities show the percentage (%) of the residues belonging to the favoured
654 (core), additionally allowed (allowed), generously allowed (general), disallowed region of the plot.
655 [b]Percentage (%) of the residues with compatibility score above zero.
656 [(c)]Data from De Rosa et al. [17].
657

Table 3. Time averaged structural properties calculated for wild-type and mutant Ig-like domains

	zebrafish		**murine**	
	WT	**V567D**	**WT**	**I591D**
Cα-RMSD (nm)	0.24(0.02)	0.19(0.02)	0.12(0.02)	0.18(0.02)
SASAtotal (nm^2)	66.14(2.07)	62.82(1.60)	53.32(1.98)	48.52(3.26)
Rg-protein (nm)	1.31(0.02)	1.31(0.01)	1.37(0.03)	1.47(0.01)

Standard deviations are given in parentheses

660 **Figure legends**
661

662 **Figure 1. Amino acid sequence alignment of zebrafish and murine Ig-like domains belonging**
663 **to the α-DG C-terminal region.** The alignment reflects the equivalence of residues in the two
664 structures. At the top is shown the location of the strands predicted by our molecular model of
665 murine α-DG [17]. The positions of point mutations (V567D and I591D for zebrafish and murine
666 DG, respectively) are shown in red.
667

668 **Figure 2. Structure and topology of wild-type and mutant zebrafish Ig-like domains belonging**
669 **to the α-DG C-terminal region.** The secondary structure elements (panel A) are named according
670 to Harpaz and Chothia [46]. The β-strands are colored according to the sheet to which they belong
671 and the N and C termini are indicated. The topology diagram of the domains is shown in panel B; β-
672 strands are shown as circles and the small helix as a triangle.
673

674 **Figure 3. Evolution of the structural properties of the Ig-like domain belonging to the α-DG**
675 **C-terminal region over time.** Cα RMSD (panel A), Solvent Accessible Surface Area (panel B),
676 and Radius of gyration (protein) (panel C) of the Ig-like domains of wild-type zebrafish (black),
677 V567D zebrafish (red), wild-type murine (green) and I591D murine (light blue).
678

679 **Figure 4. Cα-RMSF values averaged per each residue over the last 30 ns of MD trajectory.**
680 Wild-type (black) and V567D (red) zebrafish simulations are shown in panel A; wild-type (green)
681 and I591D (light blue) murine simulations are shown in panel B. Only the protein region spanning
682 the Ig-like domain is shown.
683

684 **Figure 5. Time evolution of the secondary structural elements along the MD simulation**
685 **generated by DSSP.** Wild-type zebrafish (panel A); V567D zebrafish (panel B); wild-type murine

(panel C); I591D murine (panel D). The X-axis represents the MD trajectory time (in ns), while the residue numbers are shown on the Y-axis. Only the protein region spanning the Ig-like domain is shown.

Figure 6. Backbone hydrogen bonds along the simulation trajectories for the four models. Shown is the number of backbone hydrogen bonds formed between the A' and the G strands of zebrafish (panel A) and murine (panel B) α-DG Ig-like domains. The black and gray lines show the trajectories for wild-type and mutant systems, respectively.

Figure 7. Distance analysis between the A'-G and the B-G strands. Time evolution of the distances between Cα atoms of zebrafish residue pairs 481-567 (panel A), 483-567 (panel C), 489-567 (panel E) and 491-567 (panel G) and of murine residue pairs 504-591 (panel B), 506-591 (panel D), 512-591 (panel F) and 514-591 (panel H). The black and gray lines show the trajectories for wild-type and mutant systems, respectively.

Figure 8. Structural comparison of the predicted wild-type and mutant α-DG Ig-like domains. The wild-type zebrafish (Panel A), the zebrafish V567 mutant (Panel B), the wild-type murine (Panel C) and the murine I591D mutant (Panel D) models are shown using their corresponding average structure of the last 25 ns simulation. The location of the residues described in the current study and strands A', B, C, D, E, F, and G are also labeled.

Figure 9. Recombinant expression of α-DG(485-630)I591D. The recombinant murine mutant α-DG(485-630)I591D as well as its wild-type counterpart were purified by affinity chromatography. The fractions collected after each purification step were run on the same SDS-PAGE: lane 1: total protein extract from *E. coli* cells expressing 6xHis-Trx-α-DG(485-630)I591D; lane 2: purified 6xHis-Trx-α-DG(485-630)I591D; lane 3: 6xHis-Trx-α-DG(485-630)I591D upon thrombin

712 cleavage; lane 4: purified α-DG(485-630)I591D (arrow); lane 5: purified wild-type α-DG(485-
713 630); lane 6: 6xHis-Trx-α-DG(485-630) upon thrombin cleavage; lane 7: purified 6xHis-Trx-α-
714 DG(485-630); lane 8: total protein extract from *E. coli* cells expressing wild-type 6xHis-Trx-α-
715 DG(485-630); lane 9: protein markers.
716
717 **Figure 10. I591D mutation partially prevents the post-translational cleavage of murine DG**
718 **precursor.** 293-Ebna cells were transfected with the wild-type or the mutated I591D constructs
719 both carrying a myc-tag within the C-terminal domain of α-DG and cloned into the pEGFP vector.
720 A) Immunoprecipitation with an anti-myc-antibody of wild-type and I591D α-DGs. In cells
721 transfected with wild-type DG the slightly broad band detected at 100 kDa (TOT), that is further
722 enriched upon immunoprecipitation (IP), corresponds to the mature α-DG. In cells transfected with
723 the I591D mutant an additional and prominent band is detected at 160 kDa corresponding to the
724 uncleaved DG precursor. B) Western blot of total protein extracts probed with an anti β-DG
725 antibody. The wild-type construct displays a single band at 60 kDa corresponding to the mature β-
726 DG-GFP, while I591D shows an additional band at 160 kDa corresponding to the unprocessed DG
727 precursor (asterisk). The band at 45 kDa represents the endogenous β-DG.
728
729 **Figure S1. Primary sequences and secondary structure prediction by I-TASSER.** Prediction of
730 the secondary structure of the zebrafish wild-type (panel A), zebrafish V567D (panel B), murine
731 wild-type (panel C) and murine V591D (panel D) α-DG C-terminal regions. Strands (S), α-helices
732 (H) and coils (-), as predicted by I-TASSER, are aligned with the corresponding amino acid
733 together with the confidence score. The mutation point is underlined.
734
735 **Figure S2. Evolution of the average structural properties for the three simulations of the Ig-**
736 **like domain belonging to the α-DG C-terminal region over time**. Cα RMSD (panel A), Solvent

737 Accessible Surface Area (panel B), and Radius of gyration (protein) (panel C) of the Ig-like
738 domains of wild-type zebrafish (black), V567D zebrafish (red), wild-type murine (green) and
739 I591D murine (light blue).
740
741 **Figure S3. Average Cα-rms fluctuations per residue for the three simulations.** Cα-RMSFs were
742 calculated relative to the average structure over the last 30 ns of all three wild-type (black) and
743 V567D (red) zebrafish simulations (panel A) and wild-type (green) and I591D (light blue) murine
744 simulations (panel B). Only the protein region spanning the Ig-like domain is shown.
745
746 **Figure S4. Time evolution of the secondary structural elements, along the three independent**
747 **MD simulations, generated by DSSP.** Wild-type zebrafish (panel A); V567D zebrafish (panel B);
748 wild-type murine (panel C); I591D murine (panel D). The X-axis represents the MD trajectory time
749 (in ns), while the residue numbers are shown on the Y-axis. Only the protein region spanning the
750 Ig-like domain is shown.
751
752 **Figure S5. Backbone hydrogen bonds along the simulation trajectories for the four models.**
753 The average numbers of total backbone hydrogen bonds formed between the A' and the G strands
754 of zebrafish (panel A) and murine (panel B) α-DG Ig-like domains are plotted. The black and gray
755 lines show the trajectories for wild-type and mutant systems, respectively.
756
757 **Figure S6. Distance analysis between the A'-G and the B-G strands.** Time evolution of the
758 average distances, for the three simulations, between Cα atoms of zebrafish residue pairs 481-567
759 (panel A), 483-567 (panel C), 489-567 (panel E) and 491-567 (panel G) and of murine residue
760 pairs 504-591 (panel B), 506-591 (panel D), 512-591 (panel F) and 514-591 (panel H). The black
761 and gray lines show the trajectories for wild-type and mutant systems, respectively.

Figure1
Click here to download high resolution image

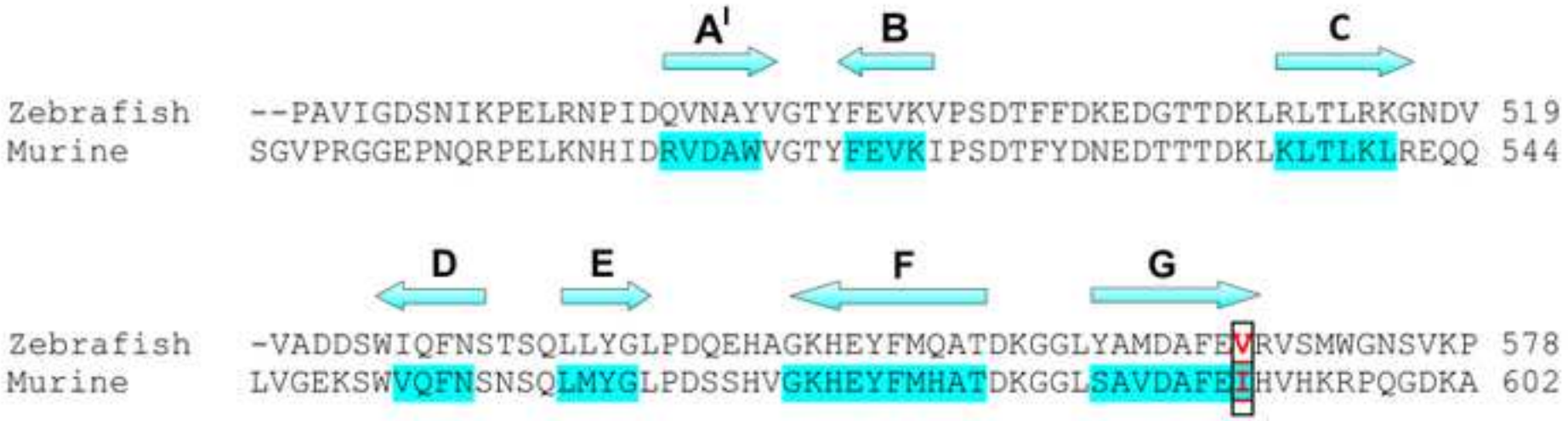

Figure2
Click here to download high resolution image

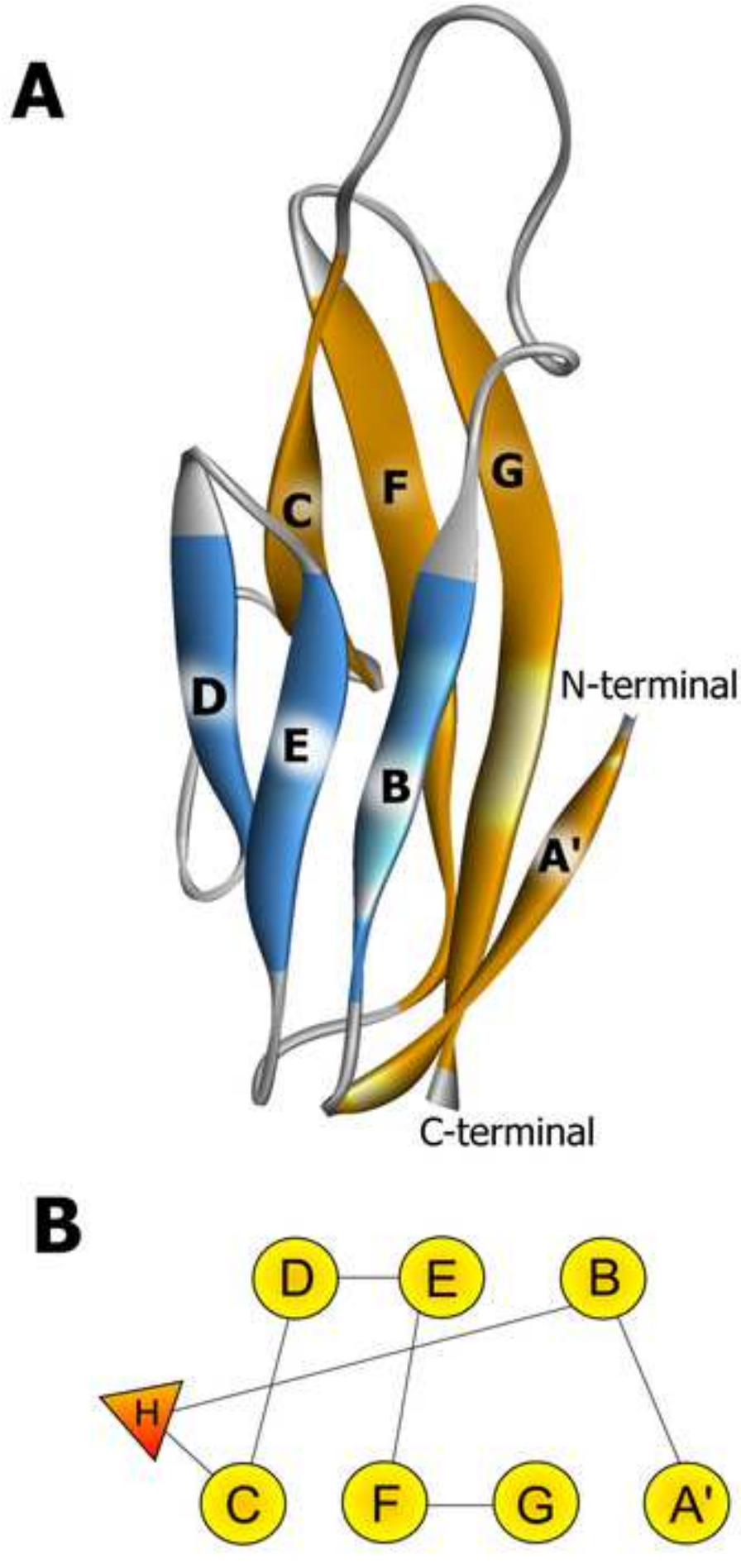

Figure3
Click here to download high resolution image

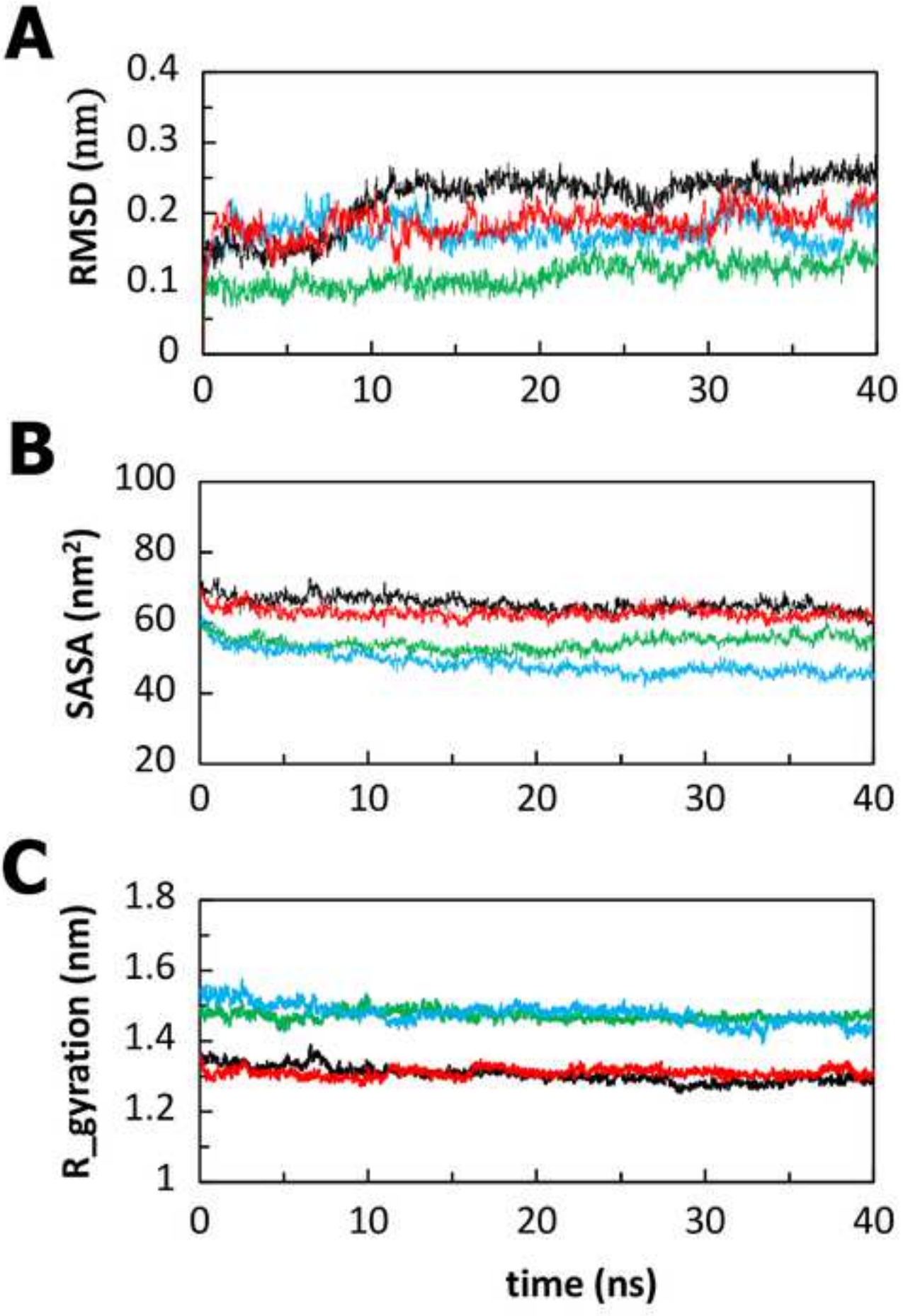

Figure4
Click here to download high resolution image

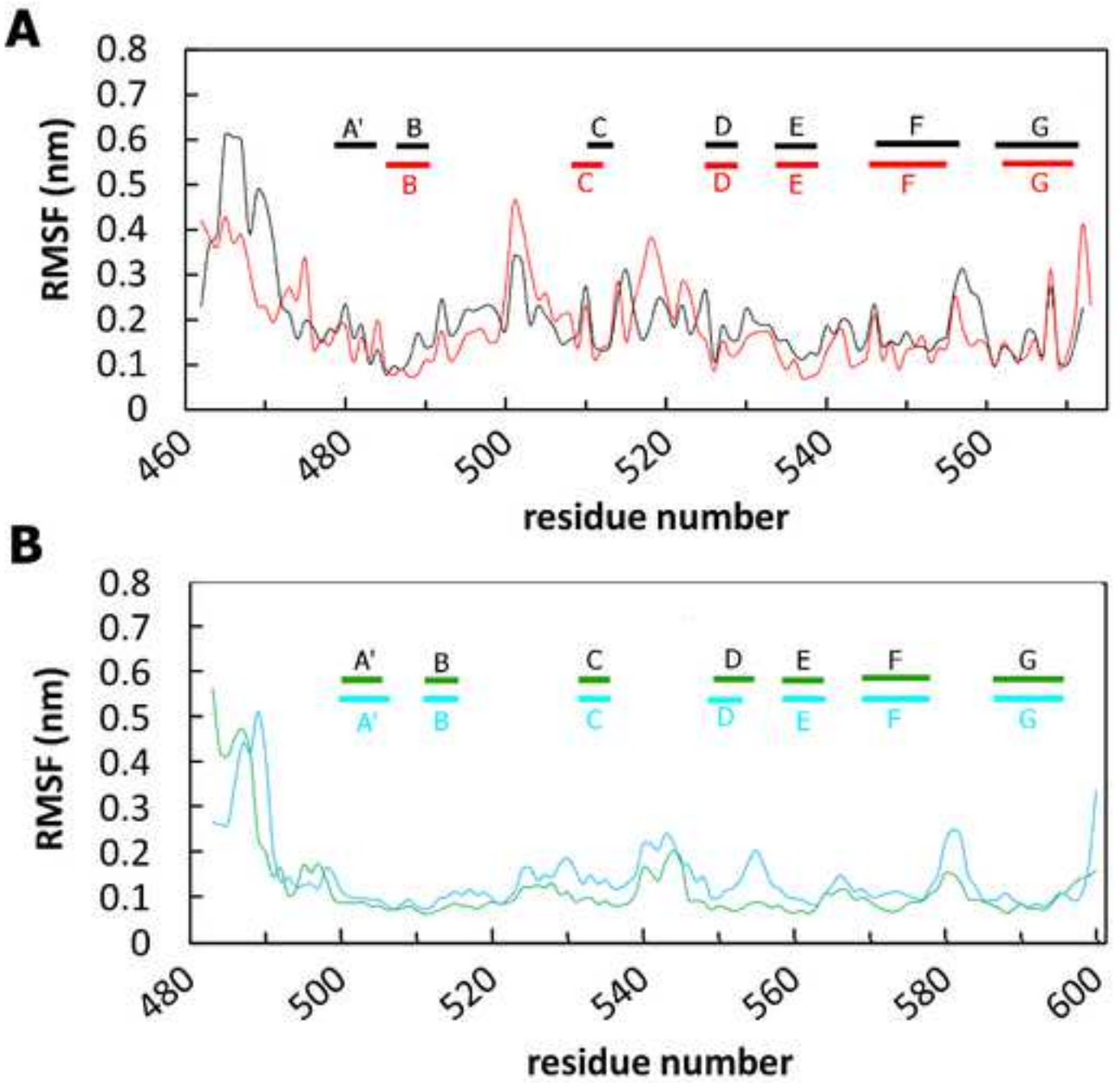

Figure5
Click here to download high resolution image

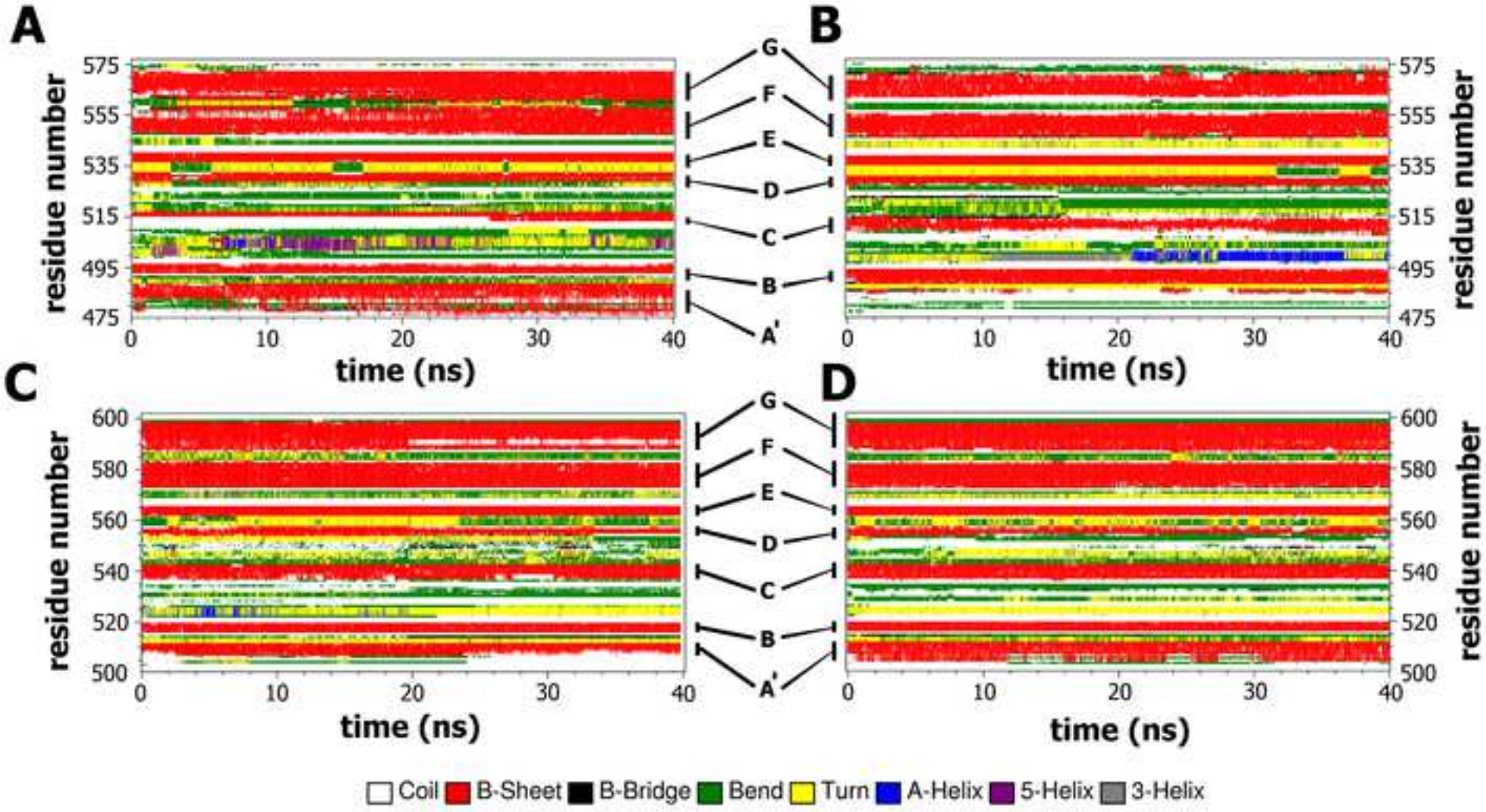

Figure6
Click here to download high resolution image

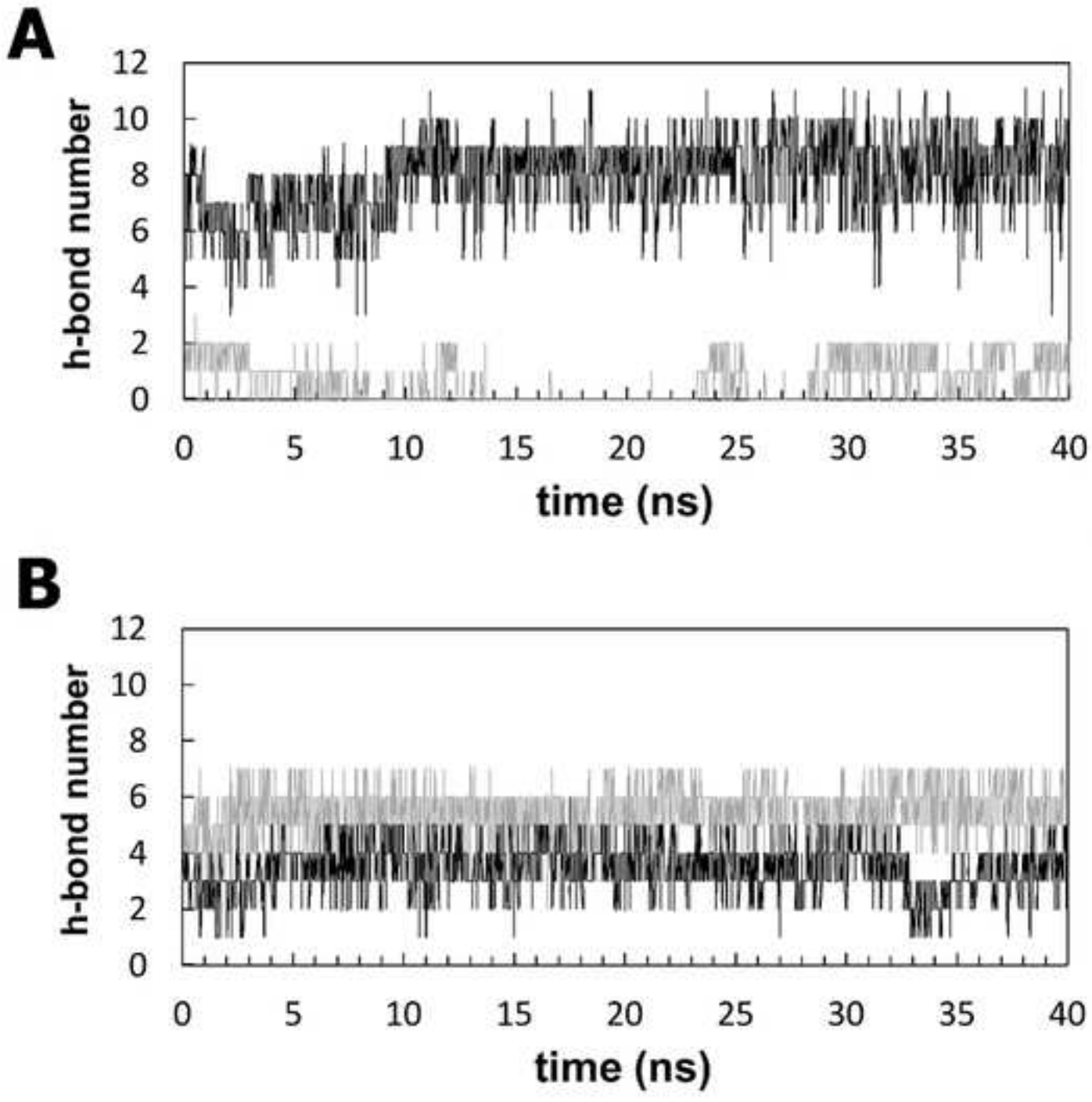

Figure7
Click here to download high resolution image

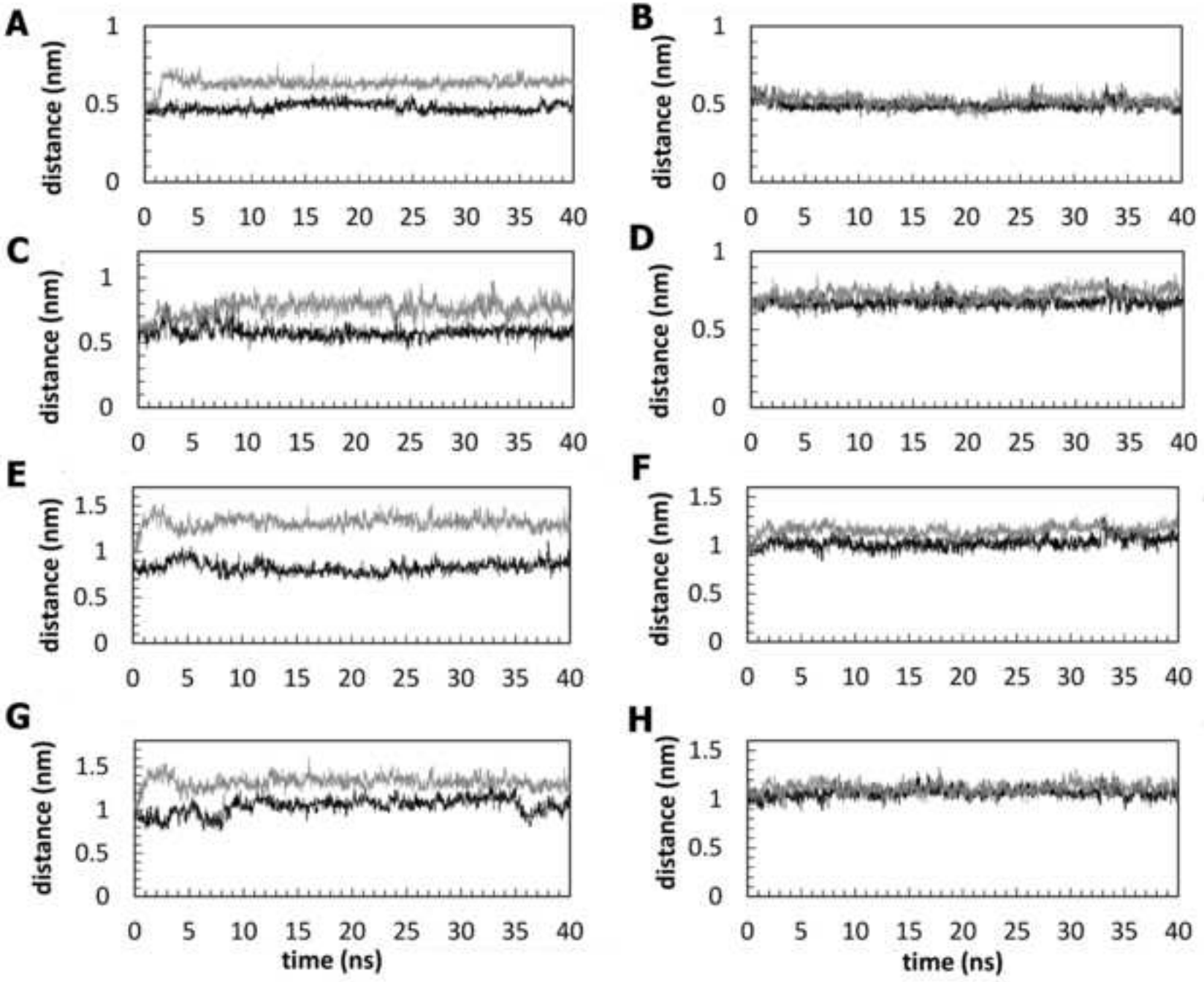

Figure8
Click here to download high resolution image

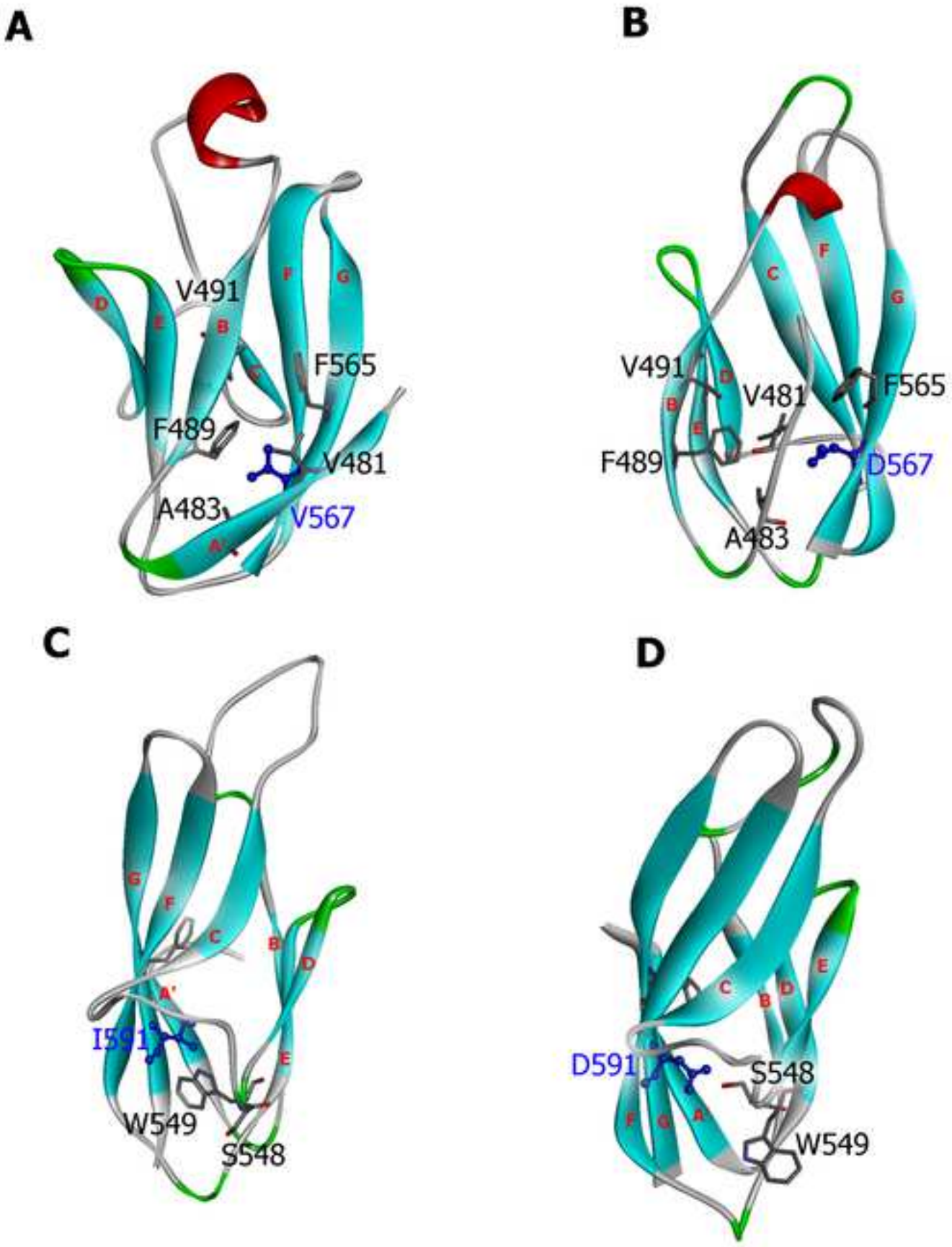

Figure9
Click here to download high resolution image

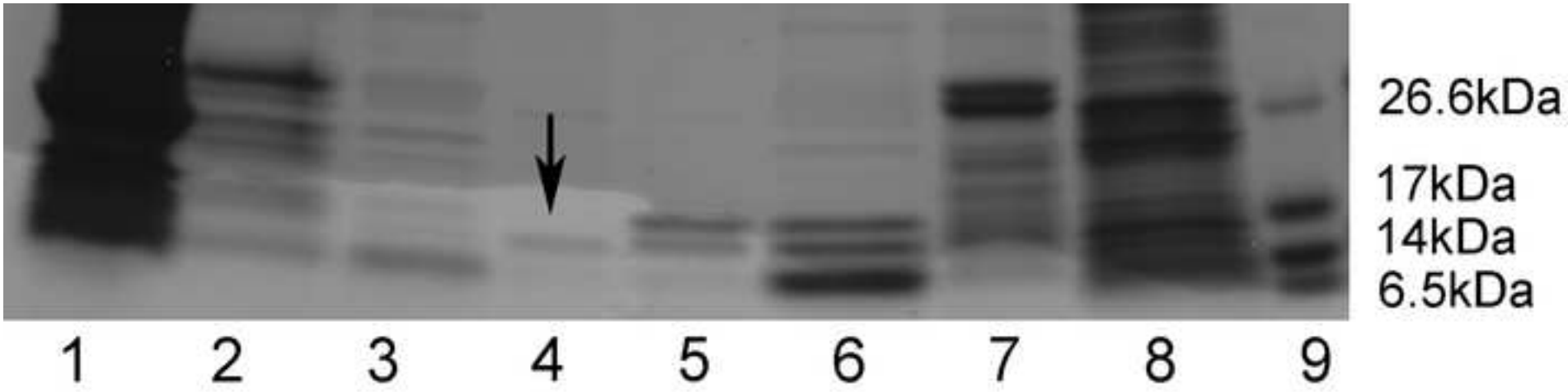

Figure10
Click here to download high resolution image

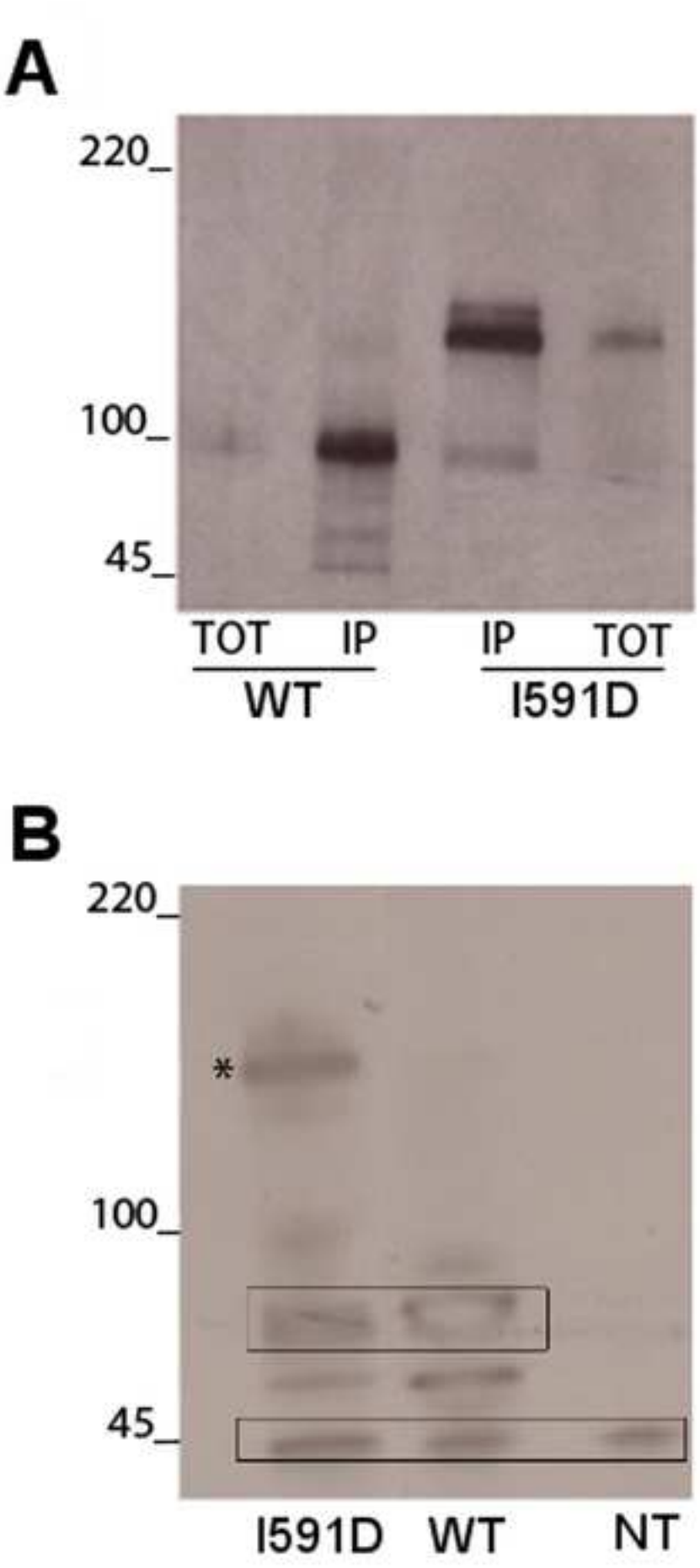

Figure S1

Click here to download Supporting Information: FigureS1.tif

Figure S2

Click here to download Supporting Information: FigureS2.tiff

Figure S3

Click here to download Supporting Information: FigureS3.tiff

Figure S4

Click here to download Supporting Information: FigureS4.tiff

Figure S5

Click here to download Supporting Information: FigureS5.tiff

Figure S6
Click here to download Supporting Information: FigureS6.tiff

Striking Image

Click here to download high resolution image

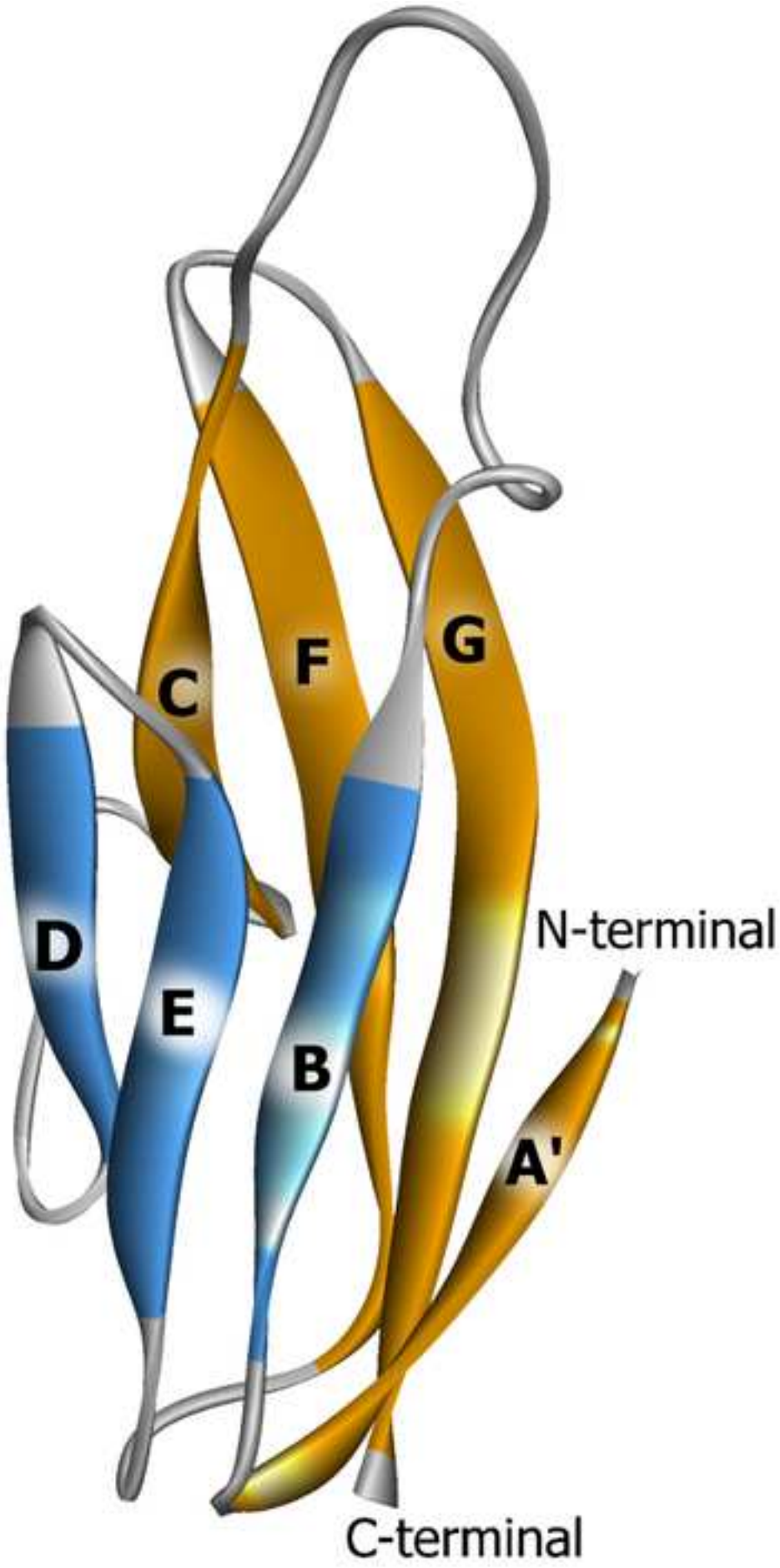

Insights from molecular dynamics simulations: structural basis for the V567D mutation-induced instability of zebrafish alpha-dystroglycan and comparison with the murine model.

Davide Pirolli[1], Francesca Sciandra[2], Manuela Bozzi[1], Bruno Giardina[1,2], Andrea Brancaccio[2*] and Maria Cristina De Rosa[2*]

[1]Istituto di Biochimica e Biochimica Clinica, Università Cattolica del Sacro Cuore and [2]Istituto di Chimica del Riconoscimento Molecolare (ICRM) - CNR c/o Università Cattolica del Sacro Cuore L.go F. Vito 1, 00168 Rome, Italy

[*]Corresponding authors contact details:

Maria Cristina De Rosa: mariacristina.derosa@icrm.cnr.it, phone: +39 06 30155135

Andrea Brancaccio: andrea.brancaccio@icrm.cnr.it, phone: +39 06 3053598

Main corresponding author: Maria Cristina De Rosa

Istituto di Chimica del Riconoscimento Molecolare - CNR

c/o Istituto di Biochimica e Biochimica Clinica, Università Cattolica del Sacro Cuore, Largo F. Vito 1, I-00168 Rome, Italy. Email: mariacristina.derosa@icrm.cnr.it.

Phone: +39 06 30155135 ; Fax: +39 06 30154309

Field Code Changed

Field Code Changed

Abstract

A missense amino acid mutation of valine to aspartic acid in 567 position of alpha-dystroglycan (DG), identified in dag1-mutated zebrafish, results in a reduced transcription and a complete absence of the protein. Lacking experimental structural data for zebrafish DG domains, the detailed mechanism for the observed mutation-induced destabilization of the DG complex and membrane damage, remained unclear. With the aim to contribute to a better clarification of ~~clarify~~ the structure-function relationships featuring the DG complex, three-dimensional structural models of wild-type and mutant (V567D) C-terminal domain of alpha-DG from zebrafish were constructed by a template-based modelling approach. We then ran extensive molecular dynamics (MD) simulations to reveal the structural and dynamic properties of the C-terminal domain and to evaluate the effect of the single mutation on alpha-DG stability. A comparative study has been also carried out on our previously generated model of murine alpha-DG C-terminal domain including the I591D mutation, which is topologically equivalent to the V567D mutation found in zebrafish. Trajectories from MD simulations were analyzed in detail, revealing extensive structural disorder involving multiple beta-strands in the mutated variant of the zebrafish protein whereas local effects have been detected in the murine protein. A biochemical analysis of the murine alpha-DG mutant I591D confirmed a pronounced instability of the protein. Taken together, the computational and biochemical analysis suggest that the V567D/I591D mutation, belonging to the G beta-strand, plays a key role in inducing a destabilization of the alpha-DG C-terminal Ig-like domain that could possibly affect and propagate to the entire DG complex. The structural features herein identified may be of crucial help to understand the molecular basis of primary dystroglycanopathies.

Introduction

Dystroglycan (DG) is a pivotal member of the dystrophin-glycoprotein complex (DGC), which links the cytoskeleton to the extracellular matrix (ECM) via dystrophin [1]. Essential for normal muscle function, DG also has important roles in a wide range of tissues, including ~~the~~ central and peripheral nervous systems, and in the maintenance of epithelial structures [2]. DG is synthesized as a precursor protein that is post-translationally cleaved into the α- and β- subunits. Within the DGC, the α-subunit is located outside the plasma membrane and binds ECM proteins, such as laminin and agrin. α-DG is extensively glycosylated and its correct glycosylation is essential to elicit its ligand binding activity [3]. Mutations in a growing number of genes encoding for glycosyltransferases or associated proteins involved in DG glycosylation give rise to a class of congenital as well as limb-girdle muscular dystrophies~~diseases~~, which are known as secondary dystroglycanopathies [4,5]. It is worthwhile to notice that, to date, only two patients affected by recessive ~~with~~ primary dystroglycanopathies, associated with mutations in the DG encoding gene *DAG1* (c.575C>T, T192M and c.2006G>T, C669FY) ~~DAG1 (c.575C>T, p.T192M and C669Y)~~ have been described [6,7].

The importance of the DG gene for muscle stability has been confirmed also in zebrafish (*Danio rerio*) [8], an organism that represents a reliable model for human muscular diseases [9–12] and that is frequently employed for investigating the effect of drugs alleviating the symptoms of Duchenne muscular dystrophy [13–15].

Recently, in an attempt to identify novel genes responsible for skeletal muscle disorders, a zebrafish mutant was identified that showed impaired locomotion behavior and dystrophic muscles [16]. Such point mutation (c.1700T>A) in *DAG1*, resulting in a missense mutation ~~p.~~V567D, induced destabilization of the DG complex and membrane damage. In particular, genetic and biochemical studies showed that the V567D substitution is associated with a strong reduction of DG transcripts and a complete absence of α and β subunits [16]. However, despite the experimental characterization of many functional effects of the V567D substitution in α-DG, a detailed molecular

Formatted: Font: Italic

Formatted: Font: Italic

framework explaining the observed destabilization and loss-of-function is stillare lacking. Comprehensive details at atomic resolution about the structural perturbations induced by the V567D substitution thus remain elusive. For this reason, and given our experience with these systems, which led us to identify a second immunoglobulin-like (Ig-like) domain in murine α-DG C-terminal region [17] and ε-sarcoglycan [18], we have exploited the capabilities of molecular dynamics (MD) simulation to investigate the structural and dynamical changes of zebrafish α-DG caused by V567D replacement. In fact, we have recently predicted and then experimentally demonstrated using recombinant proteins that not only residues 60-158 of murine α-DG display an immunoglobulinIg-like β-sandwich fold [19], but also residues ranging from ~500 to 600 [17]. We showed that the murine α-DG C-terminal is a typical β-sandwich Ig fold consisting of two β-sheets forming a β-sandwich. The first sheet contains three anti-parallel strands (B, E, D), whereas the second sheet comprises strands A', G, F and C, with A' packing parallel with the C terminus of strand G, the others arranged in an anti-parallel fashion [20]. The observed zebrafish V567D substitution [16], fallsing within a region of α-DG which that is essential for the DG complex stability, has proved to be of crucial importance to understand the role of the Ig-like domain in the interaction with the extracellular N-terminal domain of β-DG [17,21]. Gupta et al. [16], using a number of algorithms able to predict whether an amino acid substitution affects protein function, hypothesized that the V567D mutation deeply compromises protein function resulting in a pathological phenotype. Nevertheless, the structural role of this mutation remains unclear. To fill this gap, here we investigated the effects of V567D mutation on the zebrafish α-DG structure through molecular dynamics (MD) simulations, which allow the study of the conformational characteristics of the protein at every step during the computational simulations [22][21]. Subsequent structural *in silico* analyses were performed. Exploiting our murine α-DG model, we also examined the structural effects of the mutation I591D, which is topologically equivalent to the V567D mutation (Figure 1), combining computational and biochemical analysis.

Formatted: Font: Times New Roman, 12 pt, English (U.S.)

Formatted: Font: Times New Roman, 12 pt

Formatted: Font: Times New Roman, 12 pt, English (U.S.)

Formatted: Font: Calibri, 11 pt

Field Code Changed

The present MD studies revealed that the conformational stability of mutated DG is considerably reduced compared to wild-type, with a significant breakdown in the secondary structure observed for zebrafish V567D. Potential implications in processes leading to dystroglycanopathies are discussed.

Materials and Methods

Constructing structural models of wild-type and mutant α-DG C-terminal domains

Following the same procedure used in De Rosa et al. [17] the theoretical atomic models of wild-type and mutated α-DG C-terminal regions (residues 462-626 and 483-651 for zebrafish and murine proteins, respectively) were constructed using the I-TASSER server [23,24]~~[22,23]~~. Starting from the original sequence of wild-type protein retrieved from the UniProt Database [25]~~[24]~~ (accession numbers Q499B9 and Q62165 for zebrafish and murine DG, respectively), the first step I-TASSER performed was to create a sequence profile for the query using PSI-BLAST [26]~~[25]~~. The secondary structure of each of these sequences was then predicted using PSIPRED [27]~~[26]~~, a highly accurate secondary structure prediction server (http://bioinf.cs.ucl.ac.uk/psipred). Using the constraints provided by PSI-BLAST and PSIPRED, the query was then threaded through the PDB structure library using the Local Meta-Threading-Server (LOMETS) [28]~~[27]~~, which uses eight servers to find the best possible templates for the query. The continuous fragments from the threading alignments were then excised from their respective template structures and assembled into a full-length model, whereas the unmatched regions were built via *ab initio* modelling. Hence, unlike other homology modelling software, this server predicts the structure even when there are no matched sequences in known PDB~~D~~B~~D~~ structures. The quality of each predicted structure was assessed with a scoring method, and five atomistic models with the highest scores were obtained for each input protein sequence. The best models among those predicted by I-TASSER were checked using the programs PROCHECK [29]~~[28]~~, VERIFY3D [30]~~[29]~~ and ProSA-Web (https://prosa.services.came.sbg.ac.at/prosa.php) [31]~~[30]~~. Visualization and molecular graphics

Formatted: Font: Times New Roman, 12 pt, English (U.S.)
Field Code Changed
Formatted: Font: Calibri, 11 pt
Field Code Changed
Formatted: Font: Times New Roman, 12 pt, English (U.S.)
Formatted: Font: Calibri, 11 pt
Formatted: Font: Times New Roman, 12 pt, English (U.S.)
Formatted: Font: Calibri, 11 pt
Field Code Changed
Field Code Changed
Formatted: Font: Times New Roman, 12 pt, English (U.S.)
Formatted: Font: Calibri, 11 pt
Field Code Changed
Formatted: Font: Times New Roman, 12 pt, English (U.S.)
Formatted: Font: Calibri, 11 pt
Field Code Changed
Formatted: Font: Times New Roman, 12 pt
Formatted: Font: Calibri, 11 pt, Italian (Italy
Field Code Changed
Formatted: Font: Times New Roman, 12 pt, English (U.S.)
Formatted: Font: Calibri, 11 pt
Field Code Changed
Field Code Changed
Formatted: Font: Times New Roman, 12 pt, English (U.S.)
Formatted: Font: Calibri, 11 pt

were performed using Discovery Studio (Accelrys Inc.) on the workstation HP XW8600 running Red Hat Enterprice Linux 5.

Molecular Dynamics Simulations and Analysis

The best-scored wild-type and mutant DG model structures obtained by I-TASSER were chosen as the starting coordinates for the MD simulation. Calculations were performed as reported earlier [17], with slight modifications of the size and shape of the simulation box. Briefly, all simulations were carried out using the 4.5.1 version of GROMACS [32]~~[31]~~ and GROMOS96 force field [33]~~[32]~~. Each structure was immersed in a triclinic box with periodic boundary conditions. The SPC water model was used [34]~~[33]~~ and the systems were neutralized by 2 and 3 Na^+ ions (wild-type and mutant zebrafish, respectively) and by 3 and 2 Cl^- ions (wild-type and mutant murine, respectively). The box dimensions (7.3nm×5.6nm×8.5nm and 6.9nm×7.1nm×9.6nm for zebrafish and murine, respectively) were set to allow at least 0.9 nm between the protein and the box faces on each side. The final zebrafish systems consisted of 1671 (wild-type) and 1672 (V567D) protein atoms surrounded by 10725 and 10223 water molecules, respectively, whereas the final murine systems consisted of 1712 protein atoms (both wild-type and I591D) surrounded by 14999 and 14980 water molecules, respectively. All the MD simulations were carried out using periodic boundary conditions. The geometry of each system was initially optimized using the steepest descent algorithm and then equilibrated for 20 ps. Next, the molecular dynamics were run for 4~~2~~0 ns at 300 K, and the data were collected every 5 ps. Constant temperature (300 K, $\tau T = 0.1$ps) was maintained by coupling to a bath using a v-rescale algorithm [35]~~[34]~~, whereas pressure was kept at 1 atm using the Parrinello-Rahman barostat [36]~~[35]~~. Long range electrostatic interactions were calculated using the Particle-Mesh Ewald Method [37]~~[36]~~, whereas application of the Lincs method [38]~~[37]~~ allowed for an integration step size of 2 fs. Two additional replicate simulations with a duration of 40 ns were also performed for each of the systems studied, with differing initial velocities. Analysis of the trajectories was performed using the GROMACS tools g_rms, g_rmsf,

Field Code Changed
Formatted: Font: Times New Roman, 12 pt
Formatted: Font: Calibri, 11 pt, Italian (Italy
Field Code Changed
Formatted: Font: Times New Roman, 12 pt, English (U.S.)
Formatted: Font: Calibri, 11 pt
Formatted: Font: Times New Roman, 12 pt, English (U.S.)
Formatted: Font: Calibri, 11 pt
Field Code Changed
Field Code Changed
Formatted: Font: Times New Roman, 12 pt, English (U.S.)
Formatted: Font: Calibri, 11 pt
Field Code Changed
Formatted: Font: Times New Roman, 12 pt, English (U.S.)
Formatted: Font: Calibri, 11 pt
Field Code Changed
Formatted: Font: Times New Roman, 12 pt
Formatted: Font: Calibri, 11 pt, Italian (Italy
Field Code Changed
Formatted: Font: Times New Roman, 12 pt, English (U.S.)
Formatted: Font: Calibri, 11 pt

g_hbond, g_gyrate and g_sasa. Secondary structure was calculated using the DSSP algorithm [39]~~[38]~~ within GROMACS.

DNA manipulations

The single point mutation I591D was introduced into the murine DG construct containing a myc-tag inserted within the C-terminus of α-DG and cloned in pEGFP vector [40]~~[39]~~. The I591D mutation was also introduced in a DNA construct encoding for the α-DG C-terminal domain, α-DG(485-630), cloned into the pHis-Trx vector; in both cases, the QuikChange site-directed mutagenesis kit (Stratagene®) was used to introduce a mutated triplet (underlined), corresponding to an Asp residue, exploiting the following primers: I593D_S 5'-GTG GAT GCC TTC GAG GAC CAT GTT CAC AAG CGC-3'and I593D_AS 5'-GCG CTT GTG AAC ATG GTC CTC GAA GGC ATC CAC-3'. All constructs were verified by automated sequencing.

Recombinant expression and purification of α-DG(485-630)I591D

The recombinant fusion protein, 6His-Txr-α-DG(485-630), was expressed in *E.coli* BL21(DE3) Codon Plus RIL strain and purified using nickel affinity chromatography as described elsewhere [21]~~[40]~~. The protein of interest, α-DG(485-630), was obtained upon thrombin cleavage. Tricine/SDS-PAGE was used to check the purity of the recombinant protein under analysis.

Cell culture, transfection and immunoprecipitation

293-Ebna cells, grown in DMEM supplemented with antibiotics and 10 % (v/v) fetal calf serum, were transfected with 20 μg of wild-type or I591D DG constructs using the calcium phosphate method as described elsewhere [40]~~[39]~~. After 24 h, cells were dissolved in PBS containing 1% Triton X-100 and protease inhibitors (Roche, Switzerland). Cell lysate was resolved on a 10 % SDS-PAGE. For Western blot analysis, proteins were transferred to nitrocellulose and probed with an anti β-DG antibody (43-DAG) (1:50) and with a peroxidase-conjugated secondary antibody

Formatted: Font: Times New Roman, 12 pt, English (U.S.)
Field Code Changed
Formatted: Font: Calibri, 11 pt
Field Code Changed
Formatted: Font: Times New Roman, 12 pt, English (U.S.)
Formatted: Font: Calibri, 11 pt
Formatted: Font: Times New Roman, 12 pt, English (U.S.)
Formatted: Font: Calibri, 11 pt
Field Code Changed
Field Code Changed
Formatted: Font: Times New Roman, 12 pt, English (U.S.)
Formatted: Font: Calibri, 11 pt

(Sigma, USA) diluted 1:7000 (anti-mouse); the reactive products were revealed using the luminol-based ECL system (Pierce, USA).

All the steps required for immunoprecipitation were carried out using the µMACS™ Epitope Tag Protein Isolation Kit (Miltenyi Biotec.®, Germany), following the manufacturer's instructions. Briefly, 1 ml of total protein extract of transfected cells was incubated with 50 µl of magnetic beads conjugated with an anti-myc antibody (Miltenyi Biotec.®, Germany) for 30 min in ice. After several washes, the adsorbed protein was eluted with 50 µl of sample buffer and run on a 10% SDS-PAGE followed by Western blot analysis with an anti-myc antibody-HRP conjugated (Miltenyi Biotec.®, Germany).

Results and discussion

The I-TASSER approach has a high success rate to construct correct folds for medium-to-large sized proteins by structurally reassembling the fragments excised from threading template structures without using homologous templates, as demonstrated by the recent CASP experiments [41,42]. In addition, we recently demonstrated the ability of the I-TASSER server to predict a reliable model of the murine α-DG C-terminal region [17]. The I-TASSER approach was therefore used to find out the secondary and tertiary structures of zebrafish wild-type and V567D α-DG C-terminus, in comparison with the murine α-DG carrying the topologically equivalent mutation I591D. Comprehensive details at atomic resolution concerning the structural perturbations induced by these amino acid substitutions were then obtained by three statistically independent MD simulations, which allowed to refine the predicted structures within a nanosecond time scale and to investigate the conformational changes, occurring upon mutation. In total, 12 MD simulations were performed as 40 ns triplicates for zebrafish wild-type, zebrafish V567D mutant, murine wild-type and murine I591D mutant. The resulting findings are very similar for each set of the three runs and here we report the results of one of the three simulations. The average properties for the three simulations, as expected similar to those of the independent simulations are reported in the Supplemental

Information (Figures S2-S6). A graphical representation of secondary structure analysis for the three distinct MD simulations is shown (Fig. S4).

In silico modelling of zebrafish wild-type and V567D α-DG C-terminal region

In both systems, only β-strands and coils were found in the 475-574 region of α-DG, whereas coils, α helices and strands were found in the extreme C-terminus. Supplementary Figure S1 shows the predicted secondary structures of the two systems. Not surprisingly, the I-TASSER threading procedure identified immunoglobulin-like domains as the best templates for wild-type, specifically, 1U2C (α-DG N-terminal region [19]), 2WCP (mouse chaderin-23 [43]), 2YST (human protocadherin 7, to be published) and 3Q2V (mouse E-cadherin ectodomain [44]). The same templates, with the exception of 2YST were identified for the mutant V567D. The overall sequence identity shared between the α-DG C-terminal regions and each of the templates is approximately 24%. Although this value is quite low, it is similar to other cases in which modelling has been applied [45]. The quality of the generated models was assessed in I-TASSER based on two major criteria, the C- and the TM-scores. The C-score is calculated based on the significance of the threading alignments and the convergence of the I-TASSER simulations. C-scores typically range from -5 to 2, with higher scores reflecting a model of better quality. The TM-score is a measure of structural similarity between the predicted model and the native or experimentally determined structure, with a value > 0.5 indicating a model of correct topology. Assessments for the zebrafish α-DG C-terminal regions are reported in Table 1 indicating reasonable models and accurate topology. In all cases, search of the PDB, quantified by TM-score, indicated 1U2C as the structure with the highest structural similarity (Table I). As expected, the zebrafish α-DG model, as well as that of the V567D mutant, is similar in structure to the murine α-DG [17] with a root mean square deviation (RMSD) of the Cα atoms of 1.92Å (wild-type) and 1.68Å (V567D). According to I-TASSER then, the region encompassing residues 475-574 of the α-DG C-terminus adopts the typical I-frame immunoglobulin superfamily fold and is stabilized by extensive hydrophobic core

interactions between the two β-sheets [46] (Figure 2~~1~~). Consistently with the 1U2C structure and our previous results a small helix was detected between β-strands B and C (residues 495-498). The rest of the region (residues 575-626) displayed two coil-strand-coil regions separated by a helix.

To validate the computational models involved in the current study, multiple approaches were employed. Firstly, PROCHECK was used to check the stereochemistry quality and structural feature, comparing the geometry of the residues in a given protein structure with the stereochemical parameters derived from crystal or NMR structures [29]~~[28]~~. The PROCHECK result shows that 83.6% (wild-type) and 84.2% (V567D) residues are located in favored core regions, 13.0% (wild-type) and 12.3% (V567D) in allowed regions, 2.1% (wild-type) and 3.4% (V567D) in generously allowed regions and 1.4 % (wild-type) and 0.0% (V567D) in disallowed regions. For a good quality model, it is expected that the residues located in the most favorable and additional allowed regions should be more than 90%, which is the case for the computational structures of both wild-type and V567D α-DG C-terminal regions [47]. Residues Lys556 and Arg614 of wild-type were in disallowed region. It is worthwhile to remember here that both these residues are not located within secondary structure elements. Secondly, to further check the global quality of the computational model, the program VERIFY3D was used to analyze the compatibility of the residues with their environment [30]~~[29]~~. Residues with a positive score should be considered reliable. In the current case, VERIFY3D result shows that 96.4% (wild-type) and 92.1% (V567D) of the residues in our computational models has an averaged 3D-1D positive score, suggesting that the model has overall self-consistency in terms of sequence-structure compatibility. The 3D–1D profile score dips below 0 at six points in the wild-type model (from Val569 to Gly573 and Ala590) and nine points in the V567D model (from Val569 to Lys577) all belonging to the unstructured region connecting the Ig-like domain with the coil-strand-coil region. ProSA (Protein Structure Analysis) [31]~~[30]~~ was adopted to further check the quality of the generated models. The Z-scores, a parameter describing the overall model quality, are predicted to be -4.5 and -4.6 for wild-type and V567D structure model, respectively. Both values are within the range of Z-scores found for native proteins of

Formatted: Font: Times New Roman, 12 pt, English (U.S.)

Formatted: Font: Calibri, 11 pt

Field Code Changed

Field Code Changed

Formatted: Font: Times New Roman, 12 pt, English (U.S.)

Formatted: Font: Calibri, 11 pt

Formatted: Font: Times New Roman, 12 pt, English (U.S.)

Formatted: Font: Calibri, 11 pt

Field Code Changed

similar size, indicating that the overall quality of our model is high. A summary of the results obtained from these programs, indicating that the residues in the model are placed in a very good overall configuration, is reported in Table 2.

In silico modelling of murine I591D α-DG C-terminal region

Primary sequence and secondary structure prediction by I-TASSER of murine wild-type and I591D α-DG C-terminal region are shown in Supplementary Figure S1. Analogously to the zebrafish DG, only β-strands and coils were predicted in the secondary structure of the region spanning residues 500-600, whereas coils, α helices and strands were found in the extreme C-terminus. The I-TASSER server used the crystal structure of the murine α-DG N-terminal domain (PDB 1U2C [19]) and of mouse E-cadherin ectodomain (PDB 3Q2V [48]) as template structures to assemble the model of the I591D C-terminal domain of murine α-DG. Statistical support for the predicted structural models is reported in Table I. The two major criteria, the C-score and the TM-score, indicate reasonable models with very similar overall topology and a high degree of three-dimensional structure similarity. As expected, according to I-TASSER, the model of the I591D α-DG C-terminus is similar in structure to 1U2C (Cα RMSD = 1.73 Å) and consists of an Ig-like domain (residues 500–600) and a coil–helix–coil region (601-653). The structure and topology of the mutant murine Ig-like domain closely resemble those of the wild-type [17] and of the predicted zebrafish Ig-like (Figure 2~~1~~).

Analysis using PROCHECK [29]~~[28]~~ indicates excellent geometry with no residues in disallowed regions of the Ramachandran plot. 87.6%, 11.0% and 1.4% of the residues fall into the favored core, allowed, and generously allowed regions, respectively. For the most representative structure VERIFY3D and ProSA profiles also are indicative of a high quality model. In the VERIFY3D scan, the designed model shows that all the residues have an average 3D-1D positive score with the exception of Pro614, which is however located in the predicted random coil region in the extreme C-terminus. A ProSA Z-score of -4.5 also confirms the good quality of the model. Assessment of the three-dimensional model is summarized in Table 2.

Field Code Changed

Formatted: Font: Times New Roman, 12 pt, English (U.S.)

Formatted: Font: Calibri, 11 pt

Molecular dynamics conformational flexibility and stability analysis

To check the stability of the simulations, the RMSDs of the Cα atoms with respect to the minimized starting structure, radii of gyration (Rg) of the protein and Solvent Accessible Surface Area (SASA) of protein were calculated and monitored over the course of simulations and are presented in Figure 32. Evaluation of the structural drift was provided by the analysis of the Cα atom RMSDs from the initial structures as a function of time. The RMSDs of the Ig-like domains through the 420 ns trajectory were computed with respect to their corresponding initial minimized structures (Fig. 32A). In all four cases, the RMSD shows convergence of the simulation within 420 ns (Fig. 32A). The wild-type murine protein presents the smallest deviation and adopted after 200 ps a stable conformation not so far from the initial one (0.1 nm), indicating that this system was very stable during the simulation. The RMSD of wild-type zebrafish simulation converges after 10 ns to a value around 0.24 nm, whereas in the mutants simulations RMSD increases sharply till 1 ns and reaches a value of 0.20 nm (zebrafish V567D) and 0.17 nm (murine I591D) remaining reasonably stable until the end of the simulation (Fig. 32A). Figure 32 demonstrates that for all structures, the RMSD remains stable around average values of 0.1-0.2 nm (Table 3) over a considerable time period (310 ns) of the later part of the trajectory. ~~For this reason, 20 ns simulation length is believed to be a sufficient time period to sample the conformational space and evaluate the effects caused by the mutations.~~ The SASA and Rg are related to (and give a global account of~~-~~) the general tertiary structure of the protein. The curves of $SASA_{TOTAL}$ indicate that the exposed areas (both hydrophobic and hydrophilic), for all the systems investigated, although slightly decreasing with the mutation (an effect more evident in the case of zebrafish), are stable during the entire simulations (Fig. 32B). As expected from the RMSD analysis, it is not possible to observe significant changes in the Rg during the simulations. The plot of Rg versus time is presented in Fig. 32C. For both zebrafish and murine systems the curves do not differ significantly and maintain the lowest value of Rg around ~1.3 nm (zebrafish) and ~1.54 nm (murine), indicating that the compact conformation is

largely preserved upon mutation (Fig. 32C). The time averaged structural properties are reported in Table 3.

Interesting information ~~can~~ comes from the root mean square fluctuations (RMSFs) of each amino acid (Fig. 43), which highlights the flexible regions of the systems. RMSFs values higher than 0.25 nm are characteristic of amino acid residues belonging to flexible regions. For all the systems analysed, the loop at the N-terminus and the loops between the β-strands displayed RMSFs values which are typical of flexible regions, while the regular secondary structure regions showed small fluctuations during the simulations. In the zebrafish DG, the most pronounced Cα-RMSF differences between the wild-type and the mutant occur for residues 500-502 and 517-519, ~~517-524,~~ which belong to the long loops connecting strands B and C, and C and D, respectively ~~C and D, and for residues 530-533, which set up the β-turn connecting the antiparallel strands D and E~~ (Fig. 43A). In these two regions the V567D Cα-RMSF is ~1.5 and ~2 times ~~greater~~ larger ~~and lower, respectively,~~ than that of the wild-type, respectively. The RMSFs values observed for murine DG exhibit more or less similarly distributed fluctuations. Most of the residues, which belong to the ~~long~~ loops connecting strands C and D, D and E, F and G ~~strands~~, become highly mobile upon mutation (Fig. 43B).

We then tried to examine whether the mutation induced any changes in the secondary structural elements during the simulations. Fig. 54 shows the classification of the four trajectories in terms of secondary-structure elements obtained by the software tool DSSP [39] ~~[38]~~, whose plots enable a local

structural analysis complementing the above characterization of the dynamics. The stability of the secondary structures was examined during the entire period (420 ns) (Fig. 54). Interestingly, among the four simulated systems, the V567D zebrafish shows a strong disorganization of strand A' (Fig. 54B), a phenomenon not observed ~~seen~~ in the other models, whose secondary structure elements appeared very stable during the entire MD simulations. Examination of Figure 54 shows that the main features of the β-sheets structure are largely retained, i.e., the strands A', G, F, C, and the

Formatted: Font: (Default) Times New Rom

Field Code Changed

Formatted: Font: Times New Roman, 12 pt, English (U.S.)

Formatted: Font: Calibri, 11 pt

others B, E, D are preserved throughout the 420-ns simulation for wild-type zebrafish (Fig. 54A), wild-type murine (Fig. 54C) and I591D murine α-DG (Fig. 54D). By contrast, at 0.1 ns of the V567D simulation, most of the A' strand unfolds and ishas been yet converted into loop giving rise to a long flexible region at the N-terminus of the domain (Fig. 54B). Large scale fluctuations from helical to bend or turn structures at the long loop connecting strands B and C are observed in all the systems (Fig. 54).

Effects of V567D and I591D substitutions on the stability of the Ig-fold

The Ig-like domain is stabilized by hydrophobic core interactions between the two β-sheets and by the hydrogen bonds between the β-strands [39,49][38,49]. Interfering with any of the residues in the sheet by a mutation may lead to a discontinuity in the hydrogen bonding pattern, which is characteristic of the Ig-like domains. This may enhance the conformational flexibility of the mutated residue side chain, which could disrupt the natural bonding of neighbours and might result in loss of secondary structural elements [50,51]. The external strands A' and G present geometrical distortions known as β-bulges, as found in some Ig molecules [52], which lead to an imperfect general H-bond network. However, examination of the hydrogen bond patterns involving the β-strands A'-G reveals significant differences among the simulated systems (Fig. 65). Figure 65A shows that the backbone hydrogen bonds formed between the strands A' and G, where the mutation is located, are stable in zebrafish wild-type but are disrupted in the zebrafish V567D mutant, resulting in a significant separation between the two strands in the β-sheet. By contrast, the corresponding backbone hydrogen bonds in murine DG were not noticeably affected by the I591D mutation (Fig. 65B). The changes in the hydrogen bond pattern observed in zebrafish DG are closely related to the disruption of the native hydrophobic contacts. Val567 residue, located on the G strand, interacts with a number of hydrophobic residues nearby and the strongest interactions are observed with Val481(β-strand A'), Ala483(β-strand A'), Phe489 (β-strand B) and Val491 (β-strand B). Significantly, unlike Val567, the acidic Asp567 residue of mutant DG maintains its side chain

Field Code Changed

Formatted: Font: Times New Roman, 12 pt, English (U.S.)

Formatted: Font: Calibri, 11 pt

exposed to the solvent over the simulation time. Analysis of the MD trajectories shows that the hydrophobic contacts involving the 567 position remain relatively stable in the wild-type with the Val567 residue continuously interacting with residues Val481, Phe489, Ala483 and Val491 whereas they are disrupted upon mutation. This results in a significant disorganization of the A' strand and in a widening of the cleft between the sheets of the Ig-like domain. This effect is not observed in murine α-DG, in which the hydrophobic contacts established by Ile591 with Val504, Ala506, Phe512 and Val514 are well preserved after the mutation. The Cα-Cα distances between the above-mentioned residues are reported in Fig. 76 for both, zebrafish (A, C, E and G panels) and murine (B, D, F, and H panels) protein models, in comparison with their mutated counterpart. Panels A, C, E and G highlight the separation between A'-G (Fig. 76A, C) and B-G (Fig. 76E, G) strands. Notably, the large differences observed between Cα of 489, 491 (strand B) and 567 (strand A') positions (Figure 76E, G) indicate the separation between the two sheets of the β-sandwich (Fig. 21). In the case of murine α-DG the I591D replacement produces no effect on the corresponding distances between A'-G (Fig. 76B, D) strands and very little effects on the separation between the sheets (Fig. 76F, H).

We also examined the structural conformations obtained from the MD simulations of the wild-type and the mutant α-DG to better evaluate the conformational change in the mutant protein upon the amino acid replacement. Structural comparison between the average structures generated from the last 25 ns MD trajectory is shown in Figure 87. TM-score can be used as an approximate but quantitative criterion for protein topology classification, i.e. protein pairs with a TM-score >0.5 are mostly in the same fold, while those with a TM-score <0.5 are mainly not in the same fold [53,54]. A TM-score of 0.550 and 0.71 were calculated for zebrafish and murine average structures, respectively, indicative of a low similarity between the wild-type and the mutant zebrafish protein. As shown in Figure 87 the V567D substitution causes the unfolding of the A strand and the G strand pulling away from the β-sheet (Figure 87A, B). As a result, the two β-sheets slide away from each other and the average distance between the center of mass of B and G strands increases from

10.35 Å (wild-type) to 14.82 Å (V567D) (Figure 87A, B). The extent of the mutation-induced structural rearrangement can also be seen from the changes in the solvent exposure of the groups interacting with the mutation site. The segment that becomes more exposed to the solvent upon V567D mutation is the B-strand (36% SASA increase). Notably, we observed a significant increase in SASA of Val491 whose value is 14 $Å^2$ in wild-type and 32 $Å^2$ in V567D, in agreement with the analysis of Halaby and coworkers [49], who calculated, –for amino acids of the internal strand B with side chains pointing towards the interior of the protein, a SASA value < 20 $Å^2$ and for amino acids with side chains pointing towards the exterior of the protein SASA values between 20 $Å^2$ and 50 $Å^2$. In the wild-type and I591D murine average structures, we focused on the D-strand, which appears as the most affected region upon mutation. The strong hydrophobic interactions involving Ile591 and Trp549 (D strand) in wild-type murine α-DG are shown in Figure 87C. Notably, the SASA analysis shows that there is a drastic increase in SASA for Trp549, from 18 $Å^2$ (wild-type) to 45 $Å^2$ (I591D), values that are in reasonable agreement with the SASA values expected for residues of an external strand as the strand D [49]. These changes are possibly triggered by the amino acid replacement atof Ile591 position, which affected the normal interactions between Ile591 and Trp549. Effectively, in the mutant murine DG the Asp591 side chain forms an hydrogen bond with Ser548 and this results in the movement of the indole ring belonging to side chain movement of Trp549 towards the solvent (Figure 87D), an event that might induce a significant destabilization [55]. On the whole, the establishment of new contacts that remain stable during the simulation suggests that the Ig-like domain of murine α-DG should not display an impaired stability when Ile591 is replaced by Asp. Nevertheless, possible structural-functional consequences derived from the observed structural rearrangement cannot be ruled out as indicated by our analysis of the recombinant protein carrying the I591D mutation (see below).

Preparation of the recombinant murine α-DG(485-630)I591D mutant

Formatted: Font: Times New Roman, 12 pt, English (U.S.)

In order to test the stability of the mutant α-DG C-terminal domain, namely α-DG(485-630)I591D, we prepared this construct using our consolidated prokaryotic expression system (*E. coli*) that we have previously used for analyzing a plethora of murine domains of DG [21]~~[40]~~.

The recombinant mutant α-DG(485-630)I591D, expressed as a fusion protein conjugated with six N-terminal histidine residues and the thioredoxin (Trx), was purified by affinity chromatography using a nickel nitrilotriacetate resin. After thrombin cleavage to separate α-DG(485-630)I591D from its fusion partner, the protein was submitted to a further affinity chromatography step to remove the fusion partner from the solution. A similar protocol was applied to the wild-type protein in order to compare the stability of the two proteins (Fig. 9~~8~~). Any attempt made to further purify the I591D mutant was unsuccessful because of its high propensity to degradation. Figure 9~~8~~ shows an SDS-PAGE, in which protein samples at different stages of the purification protocol were analyzed. The purified protein, compared to its wild-type counterpart, displays a faint band corresponding to the lower degraded band observed in the wild-type, while no signal corresponding to the full-length protein can be observed. At the present stage, due to this pronounced unstable behavior, it is actually impossible to collect significant amounts of the I591D variant to be employed for its biochemical characterization.

Analysis of the expression of the mutant I591D in transfected 293-Ebna cells

We further assessed the effects of the I591D mutation *in vitro*, with respect to expression and post-translational processing of DG. To this end, we transiently expressed the full-length wild-type and I591D DG proteins in 293-Ebna cells using two DNA constructs carrying a myc-tag inserted at the position K498 of the C-terminal domain of α-DG and cloned in a pEGFP vector [40]~~[39]~~.

Interestingly, the mutation does not prevent or downregulate the expression of DG compared to the wild-type, however the structural rearrangements occurring in I591D partially impair the post-translational cleavage of the mutated DG precursor. In fact, an additional band at about 160 kDa is

Formatted: Font: Times New Roman, 12 pt, English (U.S.)
Field Code Changed
Formatted: Font: Calibri, 11 pt
Field Code Changed
Formatted: Font: Times New Roman, 12 pt, English (U.S.)
Formatted: Font: Calibri, 11 pt

detected in Western blot using anti β-DG or anti-myc antibodies (Fig. 10 A and B). It was already shown that mutations that affect the stability of the DG precursor, such as the disruption of disulfide bridge within the extracellular domain of β-DG or the perturbation of the interaction between the two subunits, strongly influence its post-translational cleavage and plasma membrane targeting [21,56,57].

Field Code Changed

Formatted: Font: Times New Roman, 12 pt, English (U.S.)

Formatted: Font: Calibri, 11 pt

Conclusions

Understanding the molecular consequences of the mutations that cause human genetic diseases remains an important research challenge. Missense mutations may have diverse structural and functional effects on proteins, ranging from changes in the folding pathway that may affect their overall stability, to alterations in their ligand binding properties. Computational methods have been widely used to assess the structural effects of genetic variants and to investigate the detailed mechanisms underlying the pathogenicity of missense mutations.

Given our previous biochemical and computational work on the C-terminal region of α-DG [17,21]~~[17,40]~~, it was of great interest for us that a recently discovered point mutation (c.1700T>A) in the ~~DG~~ gene *DAG1* of zebrafish, resulting in the V567D missense mutation, could induce a very strong destabilization of the protein eventually leading to the absence of protein and to a reduction of its mRNA levels [16].

In this study, the impact of the single amino acid substitution V567D on the stability of α-DG was evaluated combining a number of computational methods to improve prediction. Our findings provide new insights into the structural basis for the reported dramatic destabilization of zebrafish DG induced by the V567D mutation and gives a possible molecular explanation to understand how the homologous and topologically related I591D mutation in murine DG could also compromise the protein function. The presence of a hydrophobic residue in this position, such as a Val or Ile, is highly conserved within all the DG sequences so far analyzed [21]~~[40]. and a~~Although belonging to an external strand (G), these residues are ~~it is~~ also involved in forming hydrophobic interactions with the internal core of the Ig-like domain. We have shown that Val567 residue plays a pivotal role in maintaining the hydrophobic core structure of the Ig-like domain. By a set of molecular dynamics simulations, in which the dynamics of wild-type and mutated DG were compared, evident signs of stability loss provoked by the V567D mutation were observed in the number of hydrogen bonds, hydrophobic contacts and inter-strand packing distances between the β-sheets of the Ig-fold. The local perturbation at the G-strand may function as a nucleation site for the unfolding of the protein

Field Code Changed
Formatted: Font: Times New Roman, 12 pt, English (U.S.)
Formatted: Font: Calibri, 11 pt
Formatted: Font: Italic
Field Code Changed
Formatted: Font: Times New Roman, 12 pt, English (U.S.)
Formatted: Font: Calibri, 11 pt
Formatted: Font: Not Bold

and account for the experimentally observed destabilization [16]. We can hypothesize that in zebrafish the severe perturbation of the central hydrophobic core structure of the Ig folded-domain prevents the correct folding of the DG precursor impairing its entire maturation and targeting pathway, in line with the accepted idea that the central core of the Ig fold serves as a scaffold for the presentation of sites involved in molecular recognition, cell adhesion, and ligand binding [58,59]~~[57,58]~~.

In the case of I591D murine DG, important conformational changes were found to occur within a short time, **s**uggesting potential changes from the native structural properties within this protein region. Although we found that the I591D mutation is not likely to change the overall stability or dynamics of the entire protein region and in particular of the Ig-like domain, however, it brings about a significant local perturbation featuring the exposure of Trp549 towards the solvent. Namely, the D strand dynamics-varies in a way that may still suggest a disturbance to the structural integrity of the domain. This event may account for the reduced expression level and stability of the recombinant domain expressed in *E. coli* and the alteration of the maturation pathway observed in the transfected eukaryotic cells. On the whole, theoretical and experimental findings demonstrated that the I591D mutation can affect several biophysical characteristics simultaneously and it may therefore lead to a certain degree of instability as indicated by the high propensity to degradation displayed by the recombinant α-DG C-terminal domain (see Fig. 9~~8~~) and by the altered maturation pathway of DG, observed in our experiments using transfected cells (see Fig. 10~~9~~).

The reduced affinity displayed by hypoglycosylated DG towards laminin is believed to represent the major molecular clue behind a number of secondary dystroglycanopathies [60]~~[59]~~, while much less is currently known on the molecular mechanism behind the two known primary dystroglycanopathies [6,7]. It is interesting to note that the V567D/I591D mutation affects a domain of α-DG which is not extensively glycosylated. Only a few Thr residues within the loop interconnecting B and C strands were reported as GalNAc glycosylation sites and in particular the G strand, to which V567D/I591D belongs, was found unglycosylated [61]~~[60].~~.

Formatted: Font: Times New Roman, 12 pt, English (U.S.)

Formatted: Font: Calibri, 11 pt

Field Code Changed

Formatted: Font: Times New Roman, 12 pt, English (U.S.)

Formatted: Font: Italic

Field Code Changed

Formatted: Font: Times New Roman, 12 pt, English (U.S.)

Formatted: Font: Calibri, 11 pt

Formatted: Font: Times New Roman, 12 pt, English (U.S.)

Field Code Changed

Formatted: Font: Times New Roman, 12 pt, English (U.S.)

Formatted: Font: Calibri, 11 pt

Although we believe that the important role of this topological position within the G strand of the Ig-like domain of the C-terminal region of vertebrate dystroglycans is fully confirmed, we also believe that our analysis can be considered particularly interesting and innovative in the dystroglycan field since it is showing that even if the two orthologous proteins are highly conserved, the zebrafish background and the murine one have some obvious structural differences that in the future may be useful to define some species-specific different functional behaviours. In order to enlarge our knowledge on primary dystroglycanopathies, in the next future it will be more and more important to consider that also mutations affecting folding, stability and maturation of the DG precursor can lead to severe neuromuscular conditions ~~[7]~~ as well as those affecting DG glycosylation's shell. Our study reinforces the notion of the importance of a combined computational and biochemical approach for the study of complex diseases such as dystroglycanopathies.

Acknowledgments

The authors would like to thank Elena Gonnelli for her technical assistance.

References

1. Henry MD, Campbell KP (1999) Dystroglycan inside and out. Curr Opin Cell Biol 11: 602–607.

2. Durbeej M, Henry MD, Campbell KP (1998) Dystroglycan in development and disease. Curr Opin Cell Biol 10: 594–601.

3. Muntoni F, Torelli S, Wells DJ, Brown SC (2011) Muscular dystrophies due to glycosylation defects: diagnosis and therapeutic strategies. Curr Opin Neurol 24: 437–442. doi:10.1097/WCO.0b013e32834a95e3.

4. Muntoni F, Brockington M, Brown SC (2004) Glycosylation eases muscular dystrophy. Nat Med 10: 676–677. doi:10.1038/nm0704-676.

5. Godfrey C, Clement E, Mein R, Brockington M, Smith J, et al. (2007) Refining genotype - phenotype correlations in muscular dystrophies with defective glycosylation of dystroglycan. Brain 130: 2725–2735. doi:10.1093/Brain/Awm212.

6. Hara Y, Balci-Hayta B, Yoshida-Moriguchi T, Kanagawa M, Beltran-Valero de Bernabe D, et al. (2011) A dystroglycan mutation associated with limb-girdle muscular dystrophy. N Engl J Med 364: 939–946. doi:10.1056/NEJMoa1006939.

7. Geis T, Marquard K, Rödl T, Reihle C, Schirmer S, et al. (2013) Homozygous dystroglycan mutation associated with a novel muscle–eye–brain disease-like phenotype with multicystic leucodystrophy. neurogenetics 14: 205–213. doi:10.1007/s10048-013-0374-9.

8. Parsons MJ, Campos I, Hirst EMA, Stemple DL (2002) Removal of dystroglycan causes severe muscular dystrophy in zebrafish embryos. Dev Camb Engl 129: 3505–3512.

9. Guyon JR, Steffen LS, Howell MH, Pusack TJ, Lawrence C, et al. (2007) Modeling human muscle disease in zebrafish. Biochim Biophys Acta 1772: 205–215. doi:10.1016/j.bbadis.2006.07.003.

10. Kawahara G, Guyon JR, Nakamura Y, Kunkel LM (2010) Zebrafish models for human FKRP muscular dystrophies. Hum Mol Genet 19: 623–633. doi:10.1093/hmg/ddp528.

11. Wood AJ, Müller JS, Jepson CD, Laval SH, Lochmüller H, et al. (2011) Abnormal vascular development in zebrafish models for fukutin and FKRP deficiency. Hum Mol Genet 20: 4879–4890. doi:10.1093/hmg/ddr426.

12. Moore CJ, Goh HT, Hewitt JE (2008) Genes required for functional glycosylation of dystroglycan are conserved in zebrafish. Genomics 92: 159–167. doi:10.1016/j.ygeno.2008.05.008.

13. Winder SJ, Lipscomb L, Angela Parkin C, Juusola M (2011) The proteasomal inhibitor MG132 prevents muscular dystrophy in zebrafish. PLoS Curr 3: RRN1286. doi:10.1371/currents.RRN1286.

14. Kawahara G, Kunkel LM (2013) Zebrafish based small molecule screens for novel DMD drugs. Drug Discov Today Technol 10: e91–96. doi:10.1016/j.ddtec.2012.03.001.

Formatted: Bibliography, Automatically adju right indent when grid is defined, Widow/Orphan control, Adjust space betweer Latin and Asian text, Adjust space between Asian text and numbers

Field Code Changed

Formatted: English (U.S.)

15. Johnson NM, Farr GH 3rd, Maves L (2013) The HDAC Inhibitor TSA Ameliorates a Zebrafish Model of Duchenne Muscular Dystrophy. PLoS Curr 5. doi:10.1371/currents.md.8273cf41db10e2d15dd3ab827cb4b027.

16. Gupta V, Kawahara G, Gundry SR, Chen AT, Lencer WI, et al. (2011) The zebrafish dag1 mutant: a novel genetic model for dystroglycanopathies. Hum Mol Genet 20: 1712–1725. doi:10.1093/hmg/ddr047.

17. De Rosa MC, Pirolli D, Bozzi M, Sciandra F, Giardina B, et al. (2011) A second Ig-like domain identified in dystroglycan by molecular modelling and dynamics. J Mol Graph Model 29: 1015–1024. doi:10.1016/j.jmgm.2011.04.008.

18. Waite A, De Rosa MC, Brancaccio A, Blake DJ (2011) A gain-of-glycosylation mutation associated with myoclonus-dystonia syndrome affects trafficking and processing of mouse ε-sarcoglycan in the late secretory pathway. Hum Mutat 32: 1246–1258. doi:10.1002/humu.21561.

19. Bozic D, Sciandra F, Lamba D, Brancaccio A (2004) The structure of the N-terminal region of murine skeletal muscle alpha-dystroglycan discloses a modular architecture. J Biol Chem 279: 44812–44816. doi:10.1074/jbc.C400353200.

20. Bork P, Holm L, Sander C (1994) The immunoglobulin fold. Structural classification, sequence patterns and common core. J Mol Biol 242: 309–320. doi:10.1006/jmbi.1994.1582.

21. Sciandra F, Bozzi M, Morlacchi S, Galtieri A, Giardina B, et al. (2009) Mutagenesis at the α-β interface impairs the cleavage of the dystroglycan precursor: Mutagenesis induces an uncleaved dystroglycan. FEBS J 276: 4933–4945. doi:10.1111/j.1742-4658.2009.07196.x.

22. Daggett V, Levitt M (1993) Realistic simulations of native-protein dynamics in solution and beyond. Annu Rev Biophys Biomol Struct 22: 353–380. doi:10.1146/annurev.bb.22.060193.002033.

23. Zhang Y (2008) I-TASSER server for protein 3D structure prediction. BMC Bioinformatics 9: 40. doi:10.1186/1471-2105-9-40.

24. Wu S, Skolnick J, Zhang Y (2007) Ab initio modeling of small proteins by iterative TASSER simulations. BMC Biol 5: 17. doi:10.1186/1741-7007-5-17.

25. Jain E, Bairoch A, Duvaud S, Phan I, Redaschi N, et al. (2009) Infrastructure for the life sciences: design and implementation of the UniProt website. BMC Bioinformatics 10: 136. doi:10.1186/1471-2105-10-136.

26. Altschul SF, Madden TL, Schaffer AA, Zhang J, Zhang Z, et al. (1997) Gapped BLAST and PSI-BLAST: a new generation of protein database search programs. Nucleic Acids Res 25: 3389–3402.

27. McGuffin LJ, Bryson K, Jones DT (2000) The PSIPRED protein structure prediction server. Bioinformatics 16: 404–405.

28. Wu S, Zhang Y (2007) LOMETS: a local meta-threading-server for protein structure prediction. Nucleic Acids Res 35: 3375–3382. doi:10.1093/nar/gkm251.

Formatted: English (U.S.)

Formatted: English (U.S.)

Formatted: English (U.S.)

Formatted: English (U.S.)

Formatted: English (U.S.)

29. Morris AL, MacArthur MW, Hutchinson EG, Thornton JM (1992) Stereochemical quality of protein structure coordinates. Proteins 12: 345–364. doi:10.1002/prot.340120407.

30. Luthy R, Bowie JU, Eisenberg D (1992) Assessment of protein models with three-dimensional profiles. Nature 356: 83–85. doi:10.1038/356083a0.

31. Wiederstein M, Sippl MJ (2007) ProSA-web: interactive web service for the recognition of errors in three-dimensional structures of proteins. Nucleic Acids Res 35: W407–10. doi:10.1093/nar/gkm290.

32. Van Der Spoel D, Lindahl E, Hess B, Groenhof G, Mark AE, et al. (2005) GROMACS: fast, flexible, and free. J Comput Chem 26: 1701–1718. doi:10.1002/jcc.20291.

33. Stocker U, van Gunsteren WF (2000) Molecular dynamics simulation of hen egg white lysozyme: a test of the GROMOS96 force field against nuclear magnetic resonance data. Proteins 40: 145–153.

34. Hermans J, Berendsen HJC, Vangunsteren WF, Postma JPM (1984) A Consistent Empirical Potential for Water-Protein Interactions. Biopolymers 23: 1513–1518. doi:10.1002/bip.360230807.

35. Bussi G, Donadio D, Parrinello M (2007) Canonical sampling through velocity rescaling. J Chem Phys 126: 014101. doi:10.1063/1.2408420.

36. Parrinello M, Rahman A (1981) Polymorphic Transitions in Single-Crystals - a New Molecular-Dynamics Method. J Appl Phys 52: 7182–7190. doi:10.1063/1.328693.

37. Darden T, York D, Pedersen L (1993) Particle Mesh Ewald - an N.Log(N) Method for Ewald Sums in Large Systems. J Chem Phys 98: 10089–10092. doi:10.1063/1.464397.

38. Hess B, Bekker H, Berendsen HJC, Fraaije JGEM (1997) LINCS: A linear constraint solver for molecular simulations. J Comput Chem 18: 1463–1472. doi:10.1002/(Sici)1096-987x(199709)18:12<1463::Aid-Jcc4>3.0.Co;2-H.

39. Kabsch W, Sander C (1983) Dictionary of protein secondary structure: pattern recognition of hydrogen-bonded and geometrical features. Biopolymers 22: 2577–2637. doi:10.1002/bip.360221211.

40. Morlacchi S, Sciandra F, Bigotti M, Bozzi M, Hübner W, et al. (2012) Insertion of a myc-tag within α-dystroglycan domains improves its biochemical and microscopic detection. BMC Biochem 13: 14. doi:10.1186/1471-2091-13-14.

41. Xu D, Zhang J, Roy A, Zhang Y (2011) Automated protein structure modeling in CASP9 by I-TASSER pipeline combined with QUARK-based ab initio folding and FG-MD-based structure refinement. Proteins Struct Funct Bioinforma 79: 147–160. doi:10.1002/prot.23111.

42. Zhang Y (2013) Interplay of I-TASSER and QUARK for template-based and ab initio protein structure prediction in CASP10: Composite Protein Structure Prediction in CASP10. Proteins Struct Funct Bioinforma: n/a–n/a. doi:10.1002/prot.24341.

43. Sotomayor M, Weihofen WA, Gaudet R, Corey DP (2010) Structural determinants of cadherin-23 function in hearing and deafness. Neuron 66: 85–100. doi:10.1016/j.neuron.2010.03.028.

Formatted: English (U.S.)

Formatted: English (U.S.)

44. Harrison OJ, Jin X, Hong S, Bahna F, Ahlsen G, et al. (2011) The extracellular architecture of adherens junctions revealed by crystal structures of type I cadherins. Structure 19: 244–256. doi:10.1016/j.str.2010.11.016.

45. Bissantz C, Bernard P, Hibert M, Rognan D (2003) Protein-based virtual screening of chemical databases. II. Are homology models of G-Protein Coupled Receptors suitable targets? Proteins 50: 5–25. doi:10.1002/prot.10237.

46. Harpaz Y, Chothia C (1994) Many of the immunoglobulin superfamily domains in cell adhesion molecules and surface receptors belong to a new structural set which is close to that containing variable domains. J Mol Biol 238: 528–539. doi:10.1006/jmbi.1994.1312.

47. Wang J-F, Chou K-C (2012) Insights into the Mutation-Induced HHH Syndrome from Modeling Human Mitochondrial Ornithine Transporter-1. PLoS ONE 7: e31048. doi:10.1371/journal.pone.0031048.

48. Harrison OJ, Jin X, Hong S, Bahna F, Ahlsen G, et al. (2011) The extracellular architecture of adherens junctions revealed by crystal structures of type I cadherins. Structure 19: 244–256. doi:10.1016/j.str.2010.11.016.

49. Halaby DM, Poupon A, Mornon J-P (1999) The immunoglobulin fold family: sequence analysis and 3D structure comparisons. Protein Eng Des Sel 12: 563–571. doi:10.1093/protein/12.7.563.

50. Gajendrarao P, Krishnamoorthy N, Kassem HS, Moharem-Elgamal S, Cecchi F, et al. (2013) Molecular Modeling of Disease Causing Mutations in Domain C1 of cMyBP-C. PLoS ONE 8: e59206. doi:10.1371/journal.pone.0059206.

51. Ababou A, Rostkova E, Mistry S, Masurier CL, Gautel M, et al. (2008) Myosin Binding Protein C Positioned to Play a Key Role in Regulation of Muscle Contraction: Structure and Interactions of Domain C1. J Mol Biol 384: 615–630. doi:10.1016/j.jmb.2008.09.065.

52. Chan AW, Hutchinson EG, Harris D, Thornton JM (1993) Identification, classification, and analysis of beta-bulges in proteins. Protein Sci Publ Protein Soc 2: 1574–1590. doi:10.1002/pro.5560021004.

53. Zhang Y, Skolnick J (2004) Scoring function for automated assessment of protein structure template quality. Proteins 57: 702–710. doi:10.1002/prot.20264.

54. Xu J, Zhang Y (2010) How significant is a protein structure similarity with TM-score = 0.5? Bioinforma Oxf Engl 26: 889–895. doi:10.1093/bioinformatics/btq066.

55. Pace CN, Shirley BA, McNutt M, Gajiwala K (1996) Forces contributing to the conformational stability of proteins. FASEB J Off Publ Fed Am Soc Exp Biol 10: 75–83.

56. Watanabe N, Sasaoka T, Noguchi S, Nishino I, Tanaka T (2007) Cys669?Cys713 disulfide bridge formation is a key to dystroglycan cleavage and subunit association. Genes Cells 12: 75–88. doi:10.1111/j.1365-2443.2006.01033.x.

57. Sciandra F, Angelucci E, Altieri F, Ricci D, Hübner W, et al. (2012) Dystroglycan is associated to the disulfide isomerase ERp57. Exp Cell Res 318: 2460–2469. doi:10.1016/j.yexcr.2012.07.006.

Formatted: English (U.S.)

58. Halaby DM, Mornon JPE (1998) The immunoglobulin superfamily: An insight on its tissular, species, and functional diversity. J Mol Evol 46: 389–400. doi:10.1007/PL00006318.

59. McCormick KA (1998) Molecular Determinants of Na+ Channel Function in the Extracellular Domain of the beta 1 Subunit. J Biol Chem 273: 3954–3962. doi:10.1074/jbc.273.7.3954.

60. Sciandra F, Bozzi M, Bigotti MG, Brancaccio A (2013) The multiple affinities of α-dystroglycan. Curr Protein Pept Sci 14: 626–634.

61. Harrison R, Hitchen PG, Panico M, Morris HR, Mekhaiel D, et al. (2012) Glycoproteomic characterization of recombinant mouse α-dystroglycan. Glycobiology 22: 662–675. doi:10.1093/glycob/cws002.

1. Henry MD, Campbell KP (1999) Dystroglycan inside and out. Curr Opin Cell Biol 11: 602-607.

2. Durbeej M, Henry MD, Campbell KP (1998) Dystroglycan in development and disease. Curr Opin Cell Biol 10: 594-601.

3. Muntoni F, Torelli S, Wells DJ, Brown SC (2011) Muscular dystrophies due to glycosylation defects: diagnosis and therapeutic strategies. Curr Opin Neurol 24: 437-442.

4. Muntoni F, Brockington M, Brown SC (2004) Glycosylation eases muscular dystrophy. Nat Med 10: 676-677.

5. Godfrey C, Clement E, Mein R, Brockington M, Smith J, et al. (2007) Refining genotype - phenotype correlations in muscular dystrophies with defective glycosylation of dystroglycan. Brain 130: 2725-2735.

6. Hara Y, Balci-Hayta B, Yoshida-Moriguchi T, Kanagawa M, Beltran-Valero de Bernabe D, et al. (2011) A dystroglycan mutation associated with limb-girdle muscular dystrophy. N Engl J Med 364: 939-946.

7. Geis T, Marquard K, Rödl T, Reihle C, Schirmer S, et al. (2013) Homozygous dystroglycan mutation associated with a novel muscle–eye–brain disease-like phenotype with multicystic leucodystrophy. Neurogenetics 14: 205-213.

8. Parsons MJ, Campos I, Hirst EMA, Stemple DL (2002) Removal of dystroglycan causes severe muscular dystrophy in zebrafish embryos. Dev Camb Engl 129: 3505-3512.

9. Guyon JR, Steffen LS, Howell MH, Pusack TJ, Lawrence C, et al. (2007) Modeling human muscle disease in zebrafish. Biochim Biophys Acta 1772: 205-215.

10. Kawahara G, Guyon JR, Nakamura Y, Kunkel LM (2010) Zebrafish models for human FKRP muscular dystrophies. Hum Mol Genet 19: 623-633.

11. Wood AJ, Müller JS, Jepson CD, Laval SH, Lochmüller H, et al. (2011) Abnormal vascular development in zebrafish models for fukutin and FKRP deficiency. Hum Mol Genet 20: 4879-4890.

12. Moore CJ, Goh HT, Hewitt JE (2008) Genes required for functional glycosylation of dystroglycan are conserved in zebrafish. Genomics 92: 159-167.

13. Winder SJ, Lipscomb L, Angela Parkin C, Juusola M (2011) The proteasomal inhibitor MG132 prevents muscular dystrophy in zebrafish. PLoS Curr 3: RRN1286.

Formatted: English (U.S.)

Formatted: English (U.S.)

14. Kawahara G, Kunkel LM (2013) Zebrafish based small molecule screens for novel DMD drugs. Drug Discov Today Technol 10: e91-96.

15. Johnson NM, Farr GH 3rd, Maves L (2013) The HDAC Inhibitor TSA Ameliorates a Zebrafish Model of Duchenne Muscular Dystrophy. PLoS Curr Sep 17. Edition 1.

16. Gupta V, Kawahara G, Gundry SR, Chen AT, Lencer WI, et al. (2011) The zebrafish dag1 mutant: a novel genetic model for dystroglycanopathies. Hum Mol Genet 20: 1712-1725.

17. De Rosa MC, Pirolli D, Bozzi M, Sciandra F, Giardina B, et al. (2011) A second Ig-like domain identified in dystroglycan by molecular modelling and dynamics. J Mol Graph Model 29: 1015-1024.

18. Waite A, De Rosa MC, Brancaccio A, Blake DJ (2011) A gain-of-glycosylation mutation associated with myoclonus-dystonia syndrome affects trafficking and processing of mouse ε-sarcoglycan in the late secretory pathway. Hum Mutat 32: 1246-1258.

19. Bozic D, Sciandra F, Lamba D, Brancaccio A (2004) The structure of the N-terminal region of murine skeletal muscle alpha-dystroglycan discloses a modular architecture. J Biol Chem 279: 44812-44816.

20. Bork P, Holm L, Sander C (1994) The immunoglobulin fold. Structural classification, sequence patterns and common core. J Mol Biol 242: 309-320.

21. Daggett V, Levitt M (1993) Realistic simulations of native-protein dynamics in solution and beyond. Annu Rev Biophys Biomol Struct 22: 353-380.

22. Zhang Y (2008) I-TASSER server for protein 3D structure prediction. BMC Bioinformatics 9: 40.

23. Wu S, Skolnick J, Zhang Y (2007) Ab initio modeling of small proteins by iterative TASSER simulations. BMC Biol 5: 17.

24. Jain E, Bairoch A, Duvaud S, Phan I, Redaschi N, et al. (2009) Infrastructure for the life sciences: design and implementation of the UniProt website. BMC Bioinformatics 10: 136.

25. Altschul SF, Madden TL, Schaffer AA, Zhang J, Zhang Z, et al. (1997) Gapped BLAST and PSI-BLAST: a new generation of protein database search programs. Nucleic Acids Res 25: 3389-3402.

26. McGuffin LJ, Bryson K, Jones DT (2000) The PSIPRED protein structure prediction server. Bioinformatics 16: 404-405.

27. Wu S, Zhang Y (2007) LOMETS: a local meta-threading-server for protein structure prediction. Nucleic Acids Res 35: 3375-3382.

28. Morris AL, MacArthur MW, Hutchinson EG, Thornton JM (1992) Stereochemical quality of protein structure coordinates. Proteins 12: 345-364.

29. Luthy R, Bowie JU, Eisenberg D (1992) Assessment of protein models with three-dimensional profiles. Nature 356: 83-85.

30. Wiederstein M, Sippl MJ (2007) ProSA-web: interactive web service for the recognition of errors in three-dimensional structures of proteins. Nucleic Acids Res 35: W407-10.

31. Van Der Spoel D, Lindahl E, Hess B, Groenhof G, Mark AE, et al. (2005) GROMACS: fast, flexible, and free. J Comput Chem 26: 1701-1718.

Formatted: English (U.S.)

32. Stocker U, van Gunsteren WF (2000) Molecular dynamics simulation of hen egg white lysozyme: a test of the GROMOS96 force field against nuclear magnetic resonance data. Proteins 40: 145-153.

33. Hermans J, Berendsen HJC, Vangunsteren WF, Postma JPM (1984) A Consistent Empirical Potential for Water-Protein Interactions. Biopolymers 23: 1513-1518.

34. Bussi G, Donadio D, Parrinello M (2007) Canonical sampling through velocity rescaling. J Chem Phys 126: 014101.

35. Parrinello M, Rahman A (1981) Polymorphic Transitions in Single-Crystals - a New Molecular-Dynamics Method. J Appl Phys 52: 7182-7190.

36. Darden T, York D, Pedersen L (1993) Particle Mesh Ewald - an N.Log(N) Method for Ewald Sums in Large Systems. J Chem Phys 98: 10089-10092.

37. Hess B, Bekker H, Berendsen HJC, Fraaije JGEM (1997) LINCS: A linear constraint solver for molecular simulations. J Comput Chem 18: 1463-1472.

38. Kabsch W, Sander C (1983) Dictionary of protein secondary structure: pattern recognition of hydrogen-bonded and geometrical features. Biopolymers 22: 2577-2637.

39. Morlacchi S, Sciandra F, Bigotti M, Bozzi M, Hübner W, et al. (2012) Insertion of a myc-tag within α-dystroglycan domains improves its biochemical and microscopic detection. BMC Biochem 13: 14.

40. Sciandra F, Bozzi M, Morlacchi S, Galtieri A, Giardina B, et al. (2009) Mutagenesis at the α β interface impairs the cleavage of the dystroglycan precursor: Mutagenesis induces an uncleaved dystroglycan. FEBS J 276: 4933-4945.

41. Xu D, Zhang J, Roy A, Zhang Y (2011) Automated protein structure modeling in CASP9 by I-TASSER pipeline combined with QUARK-based ab initio folding and FG-MD-based structure refinement. Proteins Struct Funct Bioinforma 79: 147-160.

42. Zhang Y (2014) Interplay of I-TASSER and QUARK for template-based and ab initio protein structure prediction in CASP10: Composite Protein Structure Prediction in CASP10. Proteins Suppl 2:175-87.

43. Sotomayor M, Weihofen WA, Gaudet R, Corey DP (2010) Structural determinants of cadherin-23 function in hearing and deafness. Neuron 66: 85-100.

44. Harrison OJ, Jin X, Hong S, Bahna F, Ahlsen G, et al. (2011) The extracellular architecture of adherens junctions revealed by crystal structures of type I cadherins. Structure 19: 244-256.

45. Bissantz C, Bernard P, Hibert M, Rognan D (2003) Protein-based virtual screening of chemical databases. II. Are homology models of G-Protein Coupled Receptors suitable targets? Proteins 50: 5-25.

46. Harpaz Y, Chothia C (1994) Many of the immunoglobulin superfamily domains in cell adhesion molecules and surface receptors belong to a new structural set which is close to that containing variable domains. J Mol Biol 238: 528-539.

47. Wang J-F, Chou K-C (2012) Insights into the Mutation-Induced HHH Syndrome from Modeling Human Mitochondrial Ornithine Transporter-1. PLoS ONE 7: e31048.

48. Harrison OJ, Jin X, Hong S, Bahna F, Ahlsen G, et al. (2011) The extracellular architecture of adherens junctions revealed by crystal structures of type I cadherins. Structure 19: 244-256.

Formatted: English (U.S.)

Formatted: English (U.S.)

760 49. Halaby DM, Poupon A, Mornon J-P (1999) The immunoglobulin fold family: sequence analysis and 3D
761 structure comparisons. Protein Eng Des Sel 12: 563-571.

762 50. Gajendrarao P, Krishnamoorthy N, Kassem HS, Moharem-Elgamal S, Cecchi F, et al. (2013) Molecular
763 Modeling of Disease Causing Mutations in Domain C1 of cMyBP-C. PLoS ONE 8: e59206.

764 51. Ababou A, Rostkova E, Mistry S, Masurier CL, Gautel M, et al. (2008) Myosin Binding Protein C
765 Positioned to Play a Key Role in Regulation of Muscle Contraction: Structure and Interactions of
766 Domain C1. J Mol Biol 384: 615-630.

767 52. Chan AW, Hutchinson EG, Harris D, Thornton JM (1993) Identification, classification, and analysis of
768 beta-bulges in proteins. Protein Sci Publ Protein Soc 2: 1574-1590.

769 53. Zhang Y, Skolnick J (2004) Scoring function for automated assessment of protein structure template
770 quality. Proteins 57: 702-710.

771 54. Xu J, Zhang Y (2010) How significant is a protein structure similarity with TM-score = 0.5? Bioinforma
772 Oxf Engl 26: 889-895.

773 55. Watanabe N, Sasaoka T, Noguchi S, Nishino I, Tanaka T (2007) Cys669?Cys713 disulfide bridge
774 formation is a key to dystroglycan cleavage and subunit association. Genes Cells 12: 75-88.

775 56. Sciandra F, Angelucci E, Altieri F, Ricci D, Hübner W, et al. (2012) Dystroglycan is associated to the
776 disulfide isomerase ERp57. Exp Cell Res 318: 2460-2469.

777 57. Halaby DM, Mornon JPE (1998) The immunoglobulin superfamily: An insight on its tissular, species, and
778 functional diversity. J Mol Evol 46: 389-400.

779 58. McCormick KA (1998) Molecular Determinants of Na+ Channel Function in the Extracellular Domain of
780 the beta 1 Subunit. J Biol Chem 273: 3954-3962.

781 59. Sciandra F, Bozzi M, Bigotti MG, Brancaccio A (2013) The multiple affinities of α-dystroglycan. Curr
782 Protein Pept Sci 14: 626-634.

783 60. Harrison R, Hitchen PG, Panico M, Morris HR, Mekhaiel D, et al. (2012) Glycoproteomic characterization
784 of recombinant mouse α-dystroglycan. Glycobiology 22: 662-675.

Formatted: English (U.S.)

785 Table 1. Statistical support for the predicted structural models obtained from I-TASSER.

Formatted: Font: Times New Roman

α-DG	**Quality of Predicted Model**	
	C-score	**TM-Score**[a]
Wild-type zebrafish	-0.8	0.8
V567D zebrafish	-0.9	0.8
Wild type murine	-0.7	0.8
I591D murine	-0.6	0.8

786 [a]Calculated with respect to the closest structure in the PDB (1U2C)

787

Table 2. Evaluation of I-TASSER models by using PROCHECK, ProSA-Web and VERIFY3D protein structure evaluation tools.

α-DG	**PROCHECK**				**VERIFY3D**	**ProSA**
	Ramachandran plot statistics (%)[(a)]					
	Core	**Allowed**	**General**	**Disallowed**	**Compatibiliy score (%)[(b)]**	**z-score**
Wild-type zebrafish	83.6	13.0	2.1	1.4	96.4	-4.5
V567D zebrafish	84.2	12.3	3.4	-	92.1	-4.6
Wild-type murine[c]	94.5	4.8	-	-	100.0	-5.4
I591D murine	87.6	11.0	1.4	-	99.4	-4.5

[a]Ramachandran plot qualities show the percentage (%) of the residues belonging to the favoured (core), additionally allowed (allowed), generously allowed (general), disallowed region of the plot.
[b]Percentage (%) of the residues with compatibility score above zero.
[(c)]Data from De Rosa et al. [17].

Field Code Changed

795 **Table 3**. Time averaged structural properties calculated for wild-type and mutant Ig-like domains

	zebrafish		**murine**	
	WT	**V567D**	**WT**	**I591D**
Cα-RMSD (nm)	0.240(0.024)	0.198(0.02)	0.120(0.021)	0.187(0.02)
SASAtotal (nm^2)	66.1467(2.071.78)	62.823.05(1.60)	53.3245(1.9887)	48.5250.16(3.2610)
Rg-protein (nm)	1.3172(0.024)	1.3172(0.013)	1.3748(0.031)	1.479(0.012)

796 Standard deviations are given in parentheses

Figure legends

Figure 1. Amino acid sequence alignment of zebrafish and murine Ig-like domains belonging to the α-DG C-terminal region. The alignment reflects the equivalence of residues in the two structures. At the top is shown the location of the strands predicted by our molecular model of murine α-DG [17]. The positions of point mutations (V567D and I591D for zebrafish and murine DG, respectively) are shown in red.

Formatted: Font: Not Bold

Formatted: Font: Not Bold

Formatted: Font: Not Bold

Figure 21. Structure and topology of wild-type and mutant zebrafish Ig-like domains belonging to the α-DG C-terminal region. The secondary structure elements (panel A) are named according to Harpaz and Chothia [46]. The β-strands are colored according to the sheet to which they belong and the N and C termini are indicated. The topology diagram of the domains is shown in panel B; β-strands are shown as circles and the small helix as a triangle.

Figure 32. Evolution of the structural properties of the Ig-like domain belonging to the α-DG C-terminal region over time. Cα RMSD (panel A), Solvent Accessible Surface Area (panel B), and Radius of gyration (protein) (panel C) of the Ig-like domains of wild-type zebrafish (black), V567D zebrafish (red), wild-type murine (green) and I591D murine (light blue).

Figure 43. Cα-RMSF values averaged per each residue over the last 310 ns of MD trajectory. Wild-type (black) and V567D (red) zebrafish simulations are shown in panel A; wild-type (green) and I591D (light blue) murine simulations are shown in panel B. Only the protein region spanning the Ig-like domain is shown.

Figure 54. Time evolution of the secondary structural elements along the MD simulation generated by DSSP. Wild-type zebrafish (panel A); V567D zebrafish (panel B); wild-type murine

(panel C); I591D murine (panel D). The X-axis represents the MD trajectory time (in ns), while the residue numbers are shown on the Y-axis. Only the protein region spanning the Ig-like domain is shown.

Figure 6~~5~~. Backbone hydrogen bonds along the simulation trajectories for the four models. Shown is the number of backbone hydrogen bonds formed between the A' and the G strands of zebrafish (panel A) and murine (panel B) α-DG Ig-like domains. The black and gray lines show the trajectories for wild-type and mutant systems, respectively.

Figure 7~~6~~. Distance analysis between the A'-G and the B-G strands. Time evolution of the distances between Cα atoms of zebrafish residue pairs 481-567 (panel A), 483-567 (panel C), 489-567 (panel E) and 491-567 (panel G) and of murine residue pairs 504-591 (panel B), 506-591 (panel D), 512-591 (panel F) and 514-591 (panel H). The black and gray lines show the trajectories for wild-type and mutant systems, respectively.

Figure 8~~7~~. Structural comparison of the predicted wild-type and mutant ~~predicted~~ α-DG Ig-like domains. The wild-type zebrafish (Panel A), the zebrafish V567 mutant (Panel B), the wild-type murine (Panel C) and the murine I591D mutant (Panel D) models are shown using their corresponding average structure of the last 25~~5~~ ns simulation. The location of the residues described in the current study and strands A', B, C, D, E, F, and G are also labeled.

Figure 9~~8~~. Recombinant expression of α-DG(485-630)I591D. The recombinant murine mutant α-DG(485-630)I591D as well as its wild-type counterpart were purified by affinity chromatography. The fractions collected after each purification step were run on the same SDS-PAGE: lane 1: total protein extract from *E. coli* cells expressing 6xHis-Trx-α-DG(485-630)I591D; lane 2: purified 6xHis-Trx-α-DG(485-630)I591D; lane 3: 6xHis-Trx-α-DG(485-630)I591D upon thrombin

cleavage; lane 4: purified α-DG(485-630)I591D (arrow); lane 5: purified wild-type α-DG(485-630); lane 6: 6xHis-Trx-α-DG(485-630) upon thrombin cleavage; lane 7: purified 6xHis-Trx-α-DG(485-630); lane 8: total protein extract from *E. coli* cells expressing wild-type 6xHis-Trx-α-DG(485-630); lane 9: protein markers.

Figure 10~~9~~. I591D mutation partially prevents the post-translational cleavage of murine DG precursor. 293-Ebna cells were transfected with the wild-type or the mutated I591D constructs both carrying a myc-tag within the C-terminal domain of α-DG and cloned into the pEGFP vector. A) Immunoprecipitation with an anti-myc-antibody of wild-type and I591D α-DGs. In cells transfected with wild-type DG the slightly broad band detected at 100 kDa (TOT), that is further enriched upon immunoprecipitation (IP), corresponds to the mature α-DG. In cells transfected with the I591D mutant an additional and prominent band is detected at 160 kDa corresponding to the uncleaved DG precursor. B) Western blot of total protein extracts probed with an anti β-DG antibody. The wild-type construct displays a single band at 60 kDa corresponding to the mature β-DG-GFP, while I591D shows an additional band at 160 kDa corresponding to the unprocessed DG precursor (asterisk). The band at 45 kDa represents the endogenous β-DG.

Figure S1. Primary sequences and secondary structure prediction by I-TASSER. Prediction of the secondary structure of the ~~of~~ zebrafish wild-type (panel A), zebrafish V567D (panel B), murine wild-type (panel C) and murine V591D (panel D) α-DG C-terminal regions. Strands (S), α-helices (H) and coils (-), as predicted by I-TASSER, are aligned with the corresponding amino acid together with the confidence score. The mutation point is underlined.

Figure S2. Evolution of the average structural properties for the three simulations of the Ig-like domain belonging to the α-DG C-terminal region over time. Cα RMSD (panel A), Solvent

Formatted: Font: Bold

Accessible Surface Area (panel B), and Radius of gyration (protein) (panel C) of the Ig-like domains of wild-type zebrafish (black), V567D zebrafish (red), wild-type murine (green) and I591D murine (light blue).

Figure S3. Average Cα-rms fluctuations per residue for the three simulations. Cα-RMSFs were calculated relative to the average structure over the last 30 ns of all three wild-type (black) and V567D (red) zebrafish simulations (panel A) and wild-type (green) and I591D (light blue) murine simulations (panel B). Only the protein region spanning the Ig-like domain is shown.

Figure S4. Time evolution of the secondary structural elements, along the three independent MD simulations, generated by DSSP. Wild-type zebrafish (panel A); V567D zebrafish (panel B); wild-type murine (panel C); I591D murine (panel D). The X-axis represents the MD trajectory time (in ns), while the residue numbers are shown on the Y-axis. Only the protein region spanning the Ig-like domain is shown.

Figure S5. Backbone hydrogen bonds along the simulation trajectories for the four models. The average numbers of total backbone hydrogen bonds formed between the A' and the G strands of zebrafish (panel A) and murine (panel B) α-DG Ig-like domains are plotted. The black and gray lines show the trajectories for wild-type and mutant systems, respectively.

Figure S6. Distance analysis between the A'-G and the B-G strands. Time evolution of the average distances, for the three simulations, between Cα atoms of zebrafish residue pairs 481-567 (panel A), 483-567 (panel C), 489-567 (panel E) and 491-567 (panel G) and of murine residue pairs 504-591 (panel B), 506-591 (panel D), 512-591 (panel F) and 514-591 (panel H). The black and gray lines show the trajectories for wild-type and mutant systems, respectively.

Formatted: Font: Bold
Formatted: Font: Bold
Formatted: Font: Bold
Formatted: Font: Bold
Formatted: Font: Bold
Formatted: Font: Bold

Dear Editor,

Thank you very much for reviewing our manuscript (PONE-D-14-16320) which has now been completely revised according to the recommendations of the reviewers. We really appreciate your suggestions which have improved the manuscript considerably.
Please find our clarifications of all the reviewer's comments below and the specific adjustments made in the revised manuscript.
We hope that the manuscript is now suitable for publication in PLoS ONE

Kind regards

Maria Cristina De Rosa

Reviewer #1

1) "to better clarify" was changed into "a better clarification" (Line 28 of the revised manuscript).
2) As suggested by the reviewer, "Ig" definition was indicated on line 73 of the revised manuscript.
3) TM-score is a recently proposed scale for measuring the structural similarity between two structures (see Zhang and Skolnick, Scoring function for automated assessment of protein structure template quality, Proteins, 2004 57: 702-710). The purpose of proposing TM-score is to solve the problem of RMSD which is sensitive to the local error. In TM-score, the small distance is weighted stronger than the big distance which makes the score insensitive to the local modeling error. A TM-score >0.5 indicates a model of correct topology and a TM-score<0.17 means a random similarity. The TM-score values reported in Table I are parameters of the analysis performed by I-TASSER on the generated model structures. The program searches the Protein Data Bank to identify structural similarity to the predicted models and the structural similarity is quantified using TM-score. In all cases, even after the replica-exchange Monte Carlo simulations performed by I-TASSER to refine the model, 1U2C is the closest structure in the PDB and the TM-score value of 0.8 shows that the prediction is accurate.
   The meaning of the TM-score values, reported in Table I, was better explained (Lines 212-213 of the revised manuscript).
4) "2 times greater and lower" was changed (Line 304 of the revised manuscript).

Reviewer #3
Major comment:

Following the reviewer's suggestion the simulation time was doubled and an additional couple of trajectories for each protein were run (Materials and Methods of the revised manuscript, lines 141-142). This led to a significant improvement of the manuscript since our computational findings have been confirmed over three independent and longer MD simulation trajectories. It is important to outline that in the case of mutant zebrafish the observed structural

instability occurs at the first frames of the MD simulation and all the RMSD, Rg and SAS values do not significantly vary in the last 30 ns of trajectory (Lines 185-194 of the revised manuscript). For sake of clarity, in the manuscript we show the results of the original MD simulation extended to 40 ns, whereas the average properties for the three simulations and the three independent Secondary Structure trajectories are reported in the Supplemental Information (Figures S2-S6).

As far as murine DG is concerned a local rearrangement of Trp 549, that is tilted towards the solvent, has been demonstrated. This event, altering the forces which contribute to the conformational stability of the protein (Pace CN, Shirley BA, McNutt M, Gajiwala K. Forces contributing to the conformational stability of proteins. FASEB J. 1996, 10:75-83) may account for the reduced expression level and stability observed in the recombinant domain expressed in *E. coli* as well as the alteration of the maturation pathway observed in the transfected eukaryotic cells (Revised manuscript, lines 383-384).

Although we believe that the important role of this topological position within the G strand of the Ig-like domain of the C-terminal region of vertebrate dystroglycans is fully confirmed, we also believe that our analysis can be considered particularly interesting and innovative in the dystroglycan field since it is showing that even if the two orthologous proteins are highly conserved, the zebrafish background and the murine one have some obvious structural differences that in the future may be useful to define some species-specific different functional behaviours. (Revised manuscript, lines 472-478).

Minor comments:

1) As suggested by the reviewer the topologically equivalence between the I591D and V567D mutations is shown by sequence comparison in a novel Figure (Figure 1 of the revised manuscript). Figure numbering was modified accordingly.

2) In line 114 the word “PBD” was corrected as “PDB”.

3) The Rg value of zebrafish α-DG was corrected in Table 3.

4) Line 293: the Rg value of murine α-DG was corrected.

As suggested by the Editor, the manuscript has been proofread for any possible mistake and all the amendments have been reported in the marked copy.